THE ASTROPHYSICAL JOURNAL SUPPLEMENT, 107:215–226, 1996 November

AN ATLAS OF *HUBBLE SPACE TELESCOPE* ULTRAVIOLET IMAGES OF NEARBY GALAXIES[1]

DAN MAOZ,[2] ALEXEI V. FILIPPENKO,[3] LUIS C. HO,[3,4] F. DUCCIO MACCHETTO,[5]
HANS-WALTER RIX,[6] AND DONALD P. SCHNEIDER[7]

Received 1996 March 13; accepted 1996 June 13

ABSTRACT

We present an atlas of UV ($\sim$2300 Å) images, obtained with the *Hubble Space Telescope* (*HST*) Faint Object Camera, of the central 22″ × 22″ of 110 galaxies. The observed galaxies are an unbiased selection constituting about one-half of a complete sample of all large ($D > 6'$) and nearby ($V < 2000$ km s^{-1}) galaxies. This is the first extensive UV imaging survey of normal galaxies. The data are useful for studying star formation, low-level nuclear activity, and UV emission by evolved stellar populations in galaxies. At the *HST* resolution ($\sim$0.″05), the images display an assortment of morphologies and UV brightnesses. These include bright nuclear point sources, compact young star clusters scattered in the field or arranged in circumnuclear rings, centrally peaked diffuse light distributions, and galaxies with weak or undetected UV emission. We measure the integrated $\sim$2300 Å flux in each image, classify the UV morphology, and examine trends between these parameters and the optical properties of the galaxies.

Subject headings: atlases — galaxies: active — galaxies: nuclei — galaxies: star clusters — galaxies: structure — ultraviolet: galaxies

1. INTRODUCTION

Ultraviolet (UV) imaging is a powerful tool for the study of galaxies. Recent star formation and low-level nuclear activity can be traced and measured in UV images, unhindered by the bright background of the older stellar populations which dominate in visual bands. The source of UV emission in some quiescent early-type galaxies can also be studied with UV imaging. Prior to the launch of the *Hubble Space Telescope* (*HST*), few galaxies were imaged in the UV. These few were mostly Local Group spiral galaxies observed at low angular resolution using rocket-borne telescopes on brief flights (see Bohlin et al. 1990, and references therein). This situation has improved in recent years with the flight of UV imaging telescopes on the Space Shuttle (e.g., Landsman et al. 1992; Hill et al. 1992), although the angular resolution is still low and the number of galaxies observed is small, due to the limited mission duration. In this respect, *HST*, with its high sensitivity and angular resolution, has opened up a new frontier. Summaries of recent *HST* UV imaging studies of galaxies appear in Benvenuti, Macchetto, & Schreier (1996).

We have carried out a UV imaging survey with the pre-COSTAR *HST* Faint Object Camera (FOC) of the central regions of 110 large nearby galaxies, selected randomly from a complete sample of 240 galaxies. The main purposes of the survey are (1) to detect low-luminosity active galactic nuclei (AGNs), exploiting the high contrast of a nuclear UV continuum source above the low-UV background from stars, and (2) to study star formation in the central regions of the galaxies; by observing at $\sim$2300 Å, the survey images detect primarily the youngest existing stellar populations and thus provide a clean probe of the most recent sites of active star formation, uncontaminated by light from more evolved stars. The power of this technique, especially when augmented by the high *HST* angular resolution, has been recently demonstrated in UV studies of starbursts by Conti & Vacca (1994), Meurer et al. (1995), and Maoz et al. (1996).

Maoz et al. (1995) presented data from the survey for nine galaxies displaying bright compact nuclear UV sources, five of which are potential low-luminosity AGNs. Maoz et al. (1996) analyzed the images of five additional galaxies having circumnuclear star-forming rings and showed that much of the star formation in the rings is confined to massive compact clusters that are probably bound. In a forthcoming work (Ho et al. 1996b), we will use the UV images to analyze the star formation properties of all the galaxies in the sample. In this paper, we present images and basic data for the 110 galaxies observed. The images provide a reference for the UV brightness and morphology of the galaxies in the sample, which can be used as a general guide to the UV properties of the centers of galaxies and as an aid in extracting the actual data from the *HST* archive. We also provide a classification of the UV morphology, additional notes on some of the galaxies and what is seen in their images, and a measurement of the $\sim$2300 Å flux integrated over the image. We tabulate these together with the larger scale properties of the galaxies and (for the northern galaxies) the spectroscopic nuclear classification from Ho, Filippenko, & Sargent (1995, 1996a). In § 2, we describe the sample selection and the observations. In § 3 we present tables listing the galaxy parameters, a pictorial atlas of the data, and notes on some of the individual galaxies. In § 4 we compare the UV and optical properties of the galaxies and provide a brief summary.

2. OBSERVATIONS

The sample from which the observed galaxies were chosen consists of all galaxies in the UGC and ESO cata-

[1] Based on observations with the *Hubble Space Telescope* which is operated by AURA, Inc., under NASA contract NAS 5-26555.

[2] School of Physics and Astronomy and Wise Observatory, Tel-Aviv University, Tel-Aviv 69978, Israel; dani@wise.tau.ac.il.

[3] Department of Astronomy, University of California, Berkeley, CA 94720-3411.

[4] Center for Astrophysics, 60 Garden Street, Cambridge, MA 02138.

[5] Space Telescope Science Institute, 3700 San Martin Drive, Baltimore, MD 21218.

[6] Steward Observatory, University of Arizona, Tucson, AZ 85721.

[7] Department of Astronomy and Astrophysics, Pennsylvania State University, University Park, PA 16802.

logs (Lauberts & Valentijn 1989), with heliocentric velocities available in the literature and less than 2000 km s^{-1} and photographic diameters (as defined in the catalogs) greater than 6′. A total of 22 galaxies were removed from this initial sample of 262 galaxies during subsequent stages of the sample definition. In 21 of these, no nuclear position could be defined because they were too diffuse, too low in surface brightness, or edge-on with strong dust lanes. One galaxy (ESO 1331−4517) had a bright foreground star near the nucleus, which would have endangered the *HST* instruments. This left a well-defined sample of 240 galaxies with observable nuclei.

Twenty-seven galaxies from this sample were not included in our target list because they were proposed targets of other *HST* UV imaging programs. However, we have subsequently obtained from the *HST* archive the data for seven of these galaxies which were actually observed with an instrumental configuration similar to the one we used (FOC + UV filter at ∼2300 Å).

Digitized photographs from the GASP archive at Space Telescope Science Institute (STScI) of all potential target galaxies were examined and the coordinates of the nucleus determined to ∼1″–2″ precision by computing the centroid of the light distribution. In a few cases, as evidenced by the eventual *HST* images, the galaxy nucleus position was off by up to ∼5″ because of isophote distortion by dust features in the GASP images.

The observations were done in snapshot mode, i.e., targets were chosen from the target list by the STScI staff based on the convenience of their location on the sky. The brief exposure was used to fill the gaps left in the observing schedule after other science programs had been scheduled. The observed galaxies are therefore an unbiased selection from the complete sample.

Among the galaxies described in this paper, 103 were successfully observed with *HST* while the program was active, in 1993 March–July. We supplement these observations with data for the seven out of the 27 "embargoed" galaxies that were observed with *HST* between 1991 and 1995. We therefore have data for a total of 110 galaxies out of the complete sample of 240 galaxies. Observations were unsuccessful for four galaxies due to wrong coordinates (NGC 660) or telescope malfunction (NGC 3714, ESO 0514−3709, and NGC 3137); we do not count these among the successful 110 observations, even though data files for them exist in the *HST* archive.

All of our images were obtained with the *HST* f/96 FOC (Paresce 1990) in its "zoomed" 1024 × 512 pixel mode with 0.″022 × 0.″044 pixels, giving a field of view of 22″ × 22″. The F220W filter was used. This is a broadband filter with an effective wavelength of ∼2300 Å and effective bandpass of ∼500 Å. The exposure time was 10 minutes per galaxy. We will refer to this configuration and exposure time as the "standard setup." The images were processed by STScI's "pipeline" reduction (Baxter et al. 1994), after which the pixel scale is 0.″0225 $pixel^{-1}$. The data were obtained before the *HST* repair mission at the end of 1993 and therefore are affected by spherically aberrated optics. As a result, the point-spread function (PSF) consists of a sharp core of full width at half-maximum (FWHM) ∼0.″05 that contains about 15% of the light, with the rest of the light spread in a complex low-level "halo" with a radius of several arcseconds (Burrows et al. 1991). In the observing mode we have used, the FOC is limited in its dynamic range to 255 counts (8 bits) per zoomed pixel; additional signal causes the counts to "fold over" and start again from 0. Another problem is that the detected count rate becomes nonlinear, gradually saturating for bright sources (see Baxter et al. 1994). The central pixels of most of the compact bright sources detected in the images may be in the nonlinear regime, and the brightest of them are clearly saturated. In several galaxies where we report the brightness and/or angular size of individual compact sources, our analysis relies mainly on the wings of the PSF, which have low count rates ($\lesssim 0.05$ s^{-1} $pixel^{-1}$), using the algorithms described by Maoz et al. (1995, 1996). We model the PSF using a well-exposed F220W image of a star observed with the FOC f/96 256 × 256 pixel mode, which has a large dynamic and linear range (but small field of view). Such empirical PSFs are required for work in the UV (Baxter et al. 1994).

As in Maoz et al. (1995, 1996), we translate the FOC counts to a flux density f_λ at 2270 Å assuming 1 count $s^{-1} = 1.66 \times 10^{-17}$ ergs s^{-1} cm^{-2} $Å^{-1}$, based on the on-line calibration data available from STScI for the FOC and F220W filter, with a 25% increase in sensitivity of the 512 × 1024 zoomed-pixel mode relative to the 512 × 512 pixel mode (Baxter et al. 1994). This calibration assumes a spectrum that is constant in f_λ. As detailed in Maoz et al. (1995), the F220W count rate versus f_λ at 2270 Å is weakly dependent on the spectral slope, with a change of only a few percent for a large range in slopes. The uncertainty in the absolute flux is ∼20% when measuring individual compact sources (Baxter et al. 1994), but can be as small as ∼5% when measuring the UV flux integrated over large areas (e.g., ∼150 $arcsec^2$; Meurer 1995) if the background can be reliably determined.

An additional concern in UV imaging photometry is the presence of "red leaks" through the F220W filter, which we define as light of wavelength $\lambda > 3200$ Å that may pass the low, but nonzero, transmission of the filter at these wavelengths. This can be a problem when observing very red sources, e.g., the centers of the early-type galaxies in our sample. Tests by the FOC team indicate that the F220W transmission curve is not significantly changed from that measured before launch (Baxter et al. 1994), i.e., it peaks at ∼2200 Å and falls monotonically to the red, decreasing by a factor of ∼1000 between 2200 Å and 4400 Å. Using this transmission curve together with the FOC + *HST* efficiency as a function of wavelength, and the spectral energy distribution templates of early-type galaxies measured by Kinney et al. (1996), we calculate that a V-band surface brightness of 13.7 mag $arcsec^{-2}$ produces one red-leak count per dezoomed pixel in a 600 s FOC + F220W exposure. In other words, an (unrealistic) galaxy with *no* flux below 3200 Å needs to have a V surface brightness brighter than 13.7 mag $arcsec^{-2}$ in order to be detected through the red leak in our standard setup.

Lauer et al. (1995) have measured with the pre-COSTAR *HST* the V-band surface-brightness profiles of 45 nearby early-type galaxies. None of their galaxies have an observed (i.e., before deconvolution of the aberrated PSF) surface brightness brighter than 13.7 mag $arcsec^{-2}$ within a radius of 0.″1, so none would have a detected red-leak signal in our FOC exposures, even within this small (4.4 FOC pixels) radius. At a radius of 1″, where we can still detect a clear UV signal with the FOC from many of the early-type galaxies in our sample, Lauer et al. (1995) measure a surface brightness of 15 mag $arcsec^{-2}$ for the brightest galaxies in their sample,

typically 17–18 mag arcsec^{-2}. We conclude that, even without any assumptions about the shape of the spectrum at wavelengths $\lambda < 3200$ Å, the red leak contributes negligibly to the signal we detect from the reddest galaxies over most of the field of view.

We note that NGC 2997, a spiral galaxy with a circumnuclear ring, has an *HST* WFPC2 6000 Å image which Maoz et al. (1996) have analyzed in conjunction with its FOC 2300 Å image. We have convolved the 6000 Å image, which is free of spherical aberration, with the pre-COSTAR PSF and measured the surface-brightness profile. The nuclear region, which at a radius of 0".1 has a V surface brightness of 14.6 mag arcsec^{-2}, is expected to produce only 0.4 FOC counts pixel^{-1} through the F220W red leak. The nuclear region is, indeed, undetected in the UV image, as expected if the F220W transmission curve has its prelaunch values longward of 3200 Å. This comparison also sets an upper limit, of a factor of 2, by which the F220W transmission curve could be off from its prelaunch value. As a further test, we note that two of the galaxies for which Lauer et al. (1995) present V-band profiles, NGC 1023 and NGC 4636, are in our sample as well, and for both we detect with the FOC faint centrally peaked diffuse light distributions. In NGC 1023, we measure with the FOC 2.3 counts pixel^{-1} at the 0".1 radius, while Lauer et al.'s (1995) observed V-band surface brightness at this radius, of 14.8 mag arcsec^{-2} (T. Lauer 1996, private communication), is similar to that of NGC 2997, which produces no detected F220W counts. NGC 4636 has one-half as many FOC counts as NGC 1023 at 0".1, even though its observed V surface brightness is 8 times lower at this radius (T. Lauer 1996, private communication). The FOC counts for both NGC 1023 and NGC 4636 must therefore be dominated by true UV flux. This is also confirmed for NGC 1023 by the flux at 2300 Å measured with the *International Ultraviolet Explorer* (*IUE*; Kinney et al. 1993), which is consistent with the flux deduced from the FOC observation, assuming no red leak (see § 3.3).

The seven archival images which we also include in this atlas were obtained with different FOC formats, UV filters, and exposure times, providing modified fields of view, bandpasses, and sensitivities. One of these, of NGC 4151, was obtained in 1995, after the first *HST* servicing mission, and so is free of spherical aberration. We elaborate on these differences for each archival exposure in § 3.3.

3. THE ATLAS

3.1. *Tables*

The parameters of the 110 observed galaxies are listed in Table 1 (southern galaxies) and Table 2 (northern galaxies). Following is a column-by-column description of the table entries, and how they are derived.

Column (1): NGC designation of the galaxy. Footnote "a" denotes archival images, generally obtained with a different FOC format, filter, or exposure time than those of the program galaxies. See § 3.3 for details.

Column (2): UGC designation of the galaxy (northern galaxies only).

Column (3): 1950 coordinates, to 1 minute accuracy, as listed in the UGC and ESO catalogs. This datum can be useful for unambiguously identifying the galaxies in these and other catalogs, since listed coordinates for such large galaxies may vary by arcminutes from catalog to catalog. Also, some galaxies in the ESO catalog are designated solely by means of these coordinates.

Columns (4) and (5): the J2000 coordinates of the nucleus, as measured in the STScI GASP system (see § 2). These coordinates are generally accurate to $\sim$1"–2".

Column (6): V_h, the heliocentric velocity, as listed in the UGC or ESO catalogs, in km s^{-1}. The selection criterion for inclusion in the sample was $V_h < 2000$ km s^{-1}.

Columns (7) and (8): D_a, D_b, the major and minor axis diameters, in tenths of arcminutes, from the UGC and ESO catalogs. The selection criterion for inclusion in the sample was $D_a > 60$.

Column (9): $B_{\rm mag}$, the integrated B magnitude, from the UGC and ESO catalogs.

Column (10): T, the Hubble type, using de Vaucouleurs' T-type classification from the RC3 catalog (de Vaucouleurs et al. 1991). The correspondence is approximately as follows: E, -6 to -4; S0, -3 to 0 ; Sa, 1; Sb, 3; Sc, 5; Sd, 7; Irr, 10.

Column (11): Classification by Hubble type and luminosity class using the classification, when available, from the Revised Shapley-Ames Catalog of Bright Galaxies (Sandage & Tammann 1987).

Column (12): (N.B. northern galaxies only; col. [12] is absent from Table 1) Spectral classification of the nucleus, from Ho et al. (1995, 1996a). The designation is as follows: L, LINER (low-ionization nuclear emission-line region); H, H II nucleus; T, "transition" source, between LINER and H II; S, Seyfert nucleus; A, "absorption-line" nucleus with no detected emission lines. A colon denotes an uncertain classification. The Ho et al. classification is based on the Filippenko & Sargent (1985, 1986) optical spectroscopic survey of the nuclei of a flux-limited ($B < 12.5$ mag) sample of 486 northern galaxies. All but three of the northern galaxies in the *HST* survey (which is diameter- and redshift-limited) are included in the Filippenko & Sargent (1985) sample. The effective aperture of the optical observations is 2" × 4". The Ho et al. (1996a) classification is assigned after careful subtraction of absorption-line template spectra, leaving behind only the emission-line residual; see Ho et al. (1996a) for further details.

Column (13): *HST* UT observation date.

Column (14): Image rootname in the *HST* archive, useful for retrieving the actual data.

Column (15) and (16): $f_{\rm UV}$ and σ, the total f_λ(2270 Å) in units of 10^{-15} ergs s^{-1} cm^{-2} Å^{-1}, integrated above the background over the entire area of the image, and 1 σ uncertainty. The area of each image is 22" × 22", except for some of the archival exposures (marked with footnote a in col. [1]), which were taken with a different FOC format. See § 3.3 for details. The background was determined as follows. The mean counts per pixel were measured in 17 200 × 200 pixel squares in the frame, excluding occulting fingers and distortions in the FOC field (see Baxter et al. 1994), and the median counts per pixel were measured over the entire exposed part of the frame. The mean of the two lowest among these 18 measurements was used as the background value, and the standard deviation of the five lowest among the 18 measurements was used as the uncertainty in the background. The uncertainty in the background was propagated to an uncertainty on the total net counts in the image. The count rate above the background was converted to a UV flux density as described in § 2. The flux uncertainty due to the background uncertainty was combined in quadrature

TABLE 1

SOUTHERN GALAXIES

NGC (1)	Pos. 1950 (3)	R.A.(J2000) (4)	Dec.(J2000) (5)	V_h (6)	D_a (7)	D_b (8)	B_{mag} (9)	T (10)	Classif. (11)	Date (13)	Rootname (14)	f_{UV} (15)	σ (16)	Morph. (17)
24	0007–2514	0h 9m56s.47	−24°57′49″.0	560	90	17	12.10	5	Sc II-III	06/06/93	X1AR0201T	2.3	0.7	S
45	0011–2327	0 14 3.98	−23 10 51.9	468	110	80	11.20	8	Scd III	26/06/93	X1AR0301T	1.0	0.2	SW
134	0027–3331	0 30 21.53	−33 14 49.7	1581	100	20	11.00	4	Sbc II-III	22/06/93	X1AR0501T	1.3	0.1	SW
247	0044–2102	0 47 8.28	−20 45 37.0	156	300	90	9.40	7	Sc III-IV	26/06/93	X1AR0801T	3.4	0.4	PS
289	0050–3128	0 52 41.73	−31 12 28.1	1811	110	90	11.58	4	SBbc I-II	22/06/93	X1AR0A01T	1.8	0.1	SW
300	0052–3757	0 54 53.47	−37 40 60.0	145	300	200	8.70	7	Sc II.8	12/06/93	X1AR0B01T	1.9	0.3	S
908	0220–2127	2 23 4.83	−21 14 3.4	1508	80	35	10.85	5	Sc I-II	26/06/93	X1AR0Q01T	1.7	0.3	SW
...	0236–6133	2 37 49.33	−61 19 59.5	511	85	14	12.90	10	...	14/03/93	X1AR0V01T	1.8	0.3	S
1079	0241–2912	2 43 44.52	−29 0 10.4	1465	70	50	12.30	0	Sa	21/06/93	X1AR0Y01T	2.8	0.2	R
...	0255–5446	2 56 50.38	−54 34 17.1	578	90	15	11.63	7	...	27/06/93	X1AR0Z01T	1.1	0.3	SW
1232	0307–2046	3 9 45.21	−20 34 45.7	1684	95	75	10.50	5	Sc I	18/07/93	X1AR1301T	1.0	0.3	B
...	0307–4113	3 9 38.20	−41 1 56.0	950	60	30	...	8	...	23/06/93	X1AR1401T	0.9	0.3	SW
1249	0308–5331	3 10 1.29	−53 20 8.6	1007	70	40	11.80	1	SBc II	10/06/93	X1AR1501T	2.9	0.6	FSW
1291	0315–4117	3 17 18.29	−41 6 25.7	839	130	130	9.42	−3	SBa	23/06/93	X1AR1601T	2.9	0.3	F
1332	0324–2130	3 26 17.15	−21 20 4.0	1469	60	20	11.20	−3	$S0_1$	07/07/93	X1AR1C01T	2.9	0.2	F
1385	0335–2440	3 37 28.89	−24 30 7.3	1503	60	35	11.65	6	...	19/03/93	X1AR1G01T	14.9	3.3	S
1398	0336–2629	3 38 52.04	−26 20 12.8	1401	100	70	10.60	2	SBab I	12/07/93	X1AR1H01T	2.1	0.3	F
1425	0340–3003	3 42 11.39	−29 53 36.3	1510	90	40	11.70	3	Sb II	19/03/93	X1AR1J01T	1.9	0.5	F
1433	0340–4722	3 42 1.46	−47 13 19.6	1061	80	80	10.68	1	SBb I-II	21/06/93	X1AR1K01T	5.5	0.5	R
...	0344–3505	3 46 18.57	−34 56 28.4	1930	60	15	13.27	8	...	23/06/93	X1AR1N01T	1.3	0.1	SW
1512	0402–4329	4 3 54.29	−43 20 56.7	911	180	60	11.46	1	SBb I	18/07/93	X1AR1Q01T	8.4	1.8	PR
1543	0411–5751	4 12 43.01	−57 44 16.4	1088	70	70	11.57	−2	RSB0/a	04/07/93	X1AR1T01T	1.7	0.2	FP
1617	0430–5442	4 31 39.42	−54 36 6.1	1000	68	32	11.21	1	Sa	21/05/93	X1AR1X01T	1.4	0.3	F
...	0450–2519	4 52 52.95	−25 14 48.2	1374	70	50	13.24	9	...	06/07/93	X1AR1Z01T	1.2	0.2	W
1744	0457–2606	4 59 57.89	−26 1 25.9	742	160	80	11.70	7	SBcd II-III	17/04/93	X1AR2001T	1.9	0.5	SW
2442	0736–6925	7 36 23.91	−69 31 47.8	1429	60	55	11.16	3	SBbc II	02/06/93	X1AR2E01T	1.3	0.4	W
2784	0910–2358	9 12 19.29	−24 10 18.4	708	90	50	11.25	−2	$S0_1$	22/04/93	X1AR2S01T	1.5	0.2	FW
2997	0943–3057	9 45 38.65	−31 11 25.1	1081	140	130	10.32	5	Sc I.3	24/06/93	X1AR2Y01T	7.3	0.5	R
...	1033–2429	10 35 23.31	−24 45 13.1	1048	65	50	13.26	8	...	10/05/93	X1AR3901T	1.4	0.1	W
3621	1115–3232	11 18 16.06	−32 48 42.1	734	200	100	10.03	7	Sc II.8	25/07/93	X1AR3O01T	2.3	0.3	S
3717	1129–3001	11 31 31.77	−30 18 31.8	1731	80	15	12.12	3	Sb	01/06/93	X1AR3V01T	1.9	0.1	W
3981	1153–1937	11 56 7.17	−19 53 49.0	1717	120	80	12.44	4	Sbc I-II	04/05/93	X1AR4201T	1.3	0.3	B
4976	1305–4914	13 8 37.40	−49 30 20.3	1503	60	35	11.17	−5	$S0_1$	26/04/93	X1AR5B01T	2.5	0.6	FPW
5084	1317–2133	13 20 16.73	−21 49 39.1	1739	190	28	12.02	−2	$S0_1$	28/05/93	X1AR5H01T	1.2	0.3	FPW
5101	1319–2710	13 21 46.14	−27 25 47.0	1864	70	70	11.52	0	SBa	28/05/93	X1AR5I01T	1.5	0.4	FW
5102[a]	1319–3622	13 21 56.70	−36 37 52.8	420	120	50	10.35	−3	$S0_1$	02/06/93	X1CB0101T	20.2	1.3	FP
5170	1327–1742	13 29 48.78	−17 57 57.4	1498	110	16	11.88	5	Sb:	05/06/93	X1AR5K01T	0.8	0.4	B
5247	1335–1737	13 38 2.62	−17 53 1.6	1354	60	60	11.10	4	Sc I-II	09/06/93	X1AR5O01T	5.7	0.5	S
5253[a]	1337–3123	13 39 56.80	−31 38 40.8	417	60	20	10.99	0	Amorph.	21/02/93	X19P0701M	95.4	6.2	S
...	1348–3333	13 51 19.30	−33 48 28.3	1388	80	50	...	8	...	02/06/93	X1AR5R01T	1.0	0.3	W
...	2159–5132	22 2 41.90	−51 17 44.0	121	60	40	11.20	10	...	31/05/93	X1AR6N01T	10.2	1.0	S
7410	2252–3955	22 54 59.43	−39 39 44.3	1638	70	20	11.30	1	SBa	02/06/93	X1AR6T01T	1.4	0.3	B
7424	2254–4120	22 57 18.55	−41 4 13.7	951	160	160	10.99	6	Sc/Sbc II.3	03/06/93	X1AR6V01T	4.1	0.2	S
7456	2259–3950	23 2 10.11	−39 34 10.7	1211	80	26	12.06	6	Sc II-III	01/06/93	X1AR6W01T	1.0	0.3	W
7462	2260–4106	23 2 46.55	−40 50 6.5	1074	65	11	12.79	5	SBc	02/06/93	X1AR6X01T	9.0	1.3	S
7531	2312–4352	23 14 48.40	−43 35 59.7	1598	70	27	11.97	4	Sbc I-II	25/07/93	X1AR6Y01T	1.9	0.4	W
...	2331–3622	23 34 27.40	−36 6 4.9	707	140	130	11.25	7	...	05/06/93	X1AR7001T	1.3	0.3	S
...	2333–3903	23 36 27.20	−38 46 58.2	1553	60	30	...	8	...	30/05/93	X1AR7201T	1.1	0.2	PW

NOTES TO TABLE 1.—See § 3.1 for explanations of Table entries. Footnote "a" next to the galaxy NGC number denotes archival images, generally obtained with a different FOC format, filter, or exposure time than those of the program galaxies; see § 3.3 for details.

TABLE 2

NORTHERN GALAXIES

NGC (1)	UGC (2)	Pos. 1950 (3)	R.A.(J2000) (4)	Dec.(J2000) (5)	V_h (6)	D_a (7)	D_b (8)	B_{mag} (9)	T (10)	Classif. (11)	Sp. (12)	Date (13)	Rootname (14)	f_{UV} (15)	σ (16)	Morph. (17)
7814	8	0000+1552	$0^h\ 3^m14^s.93$	16° 8′43″.5	1050	65	27	12.00	2	S(ab)	L:	30/06/93	X1AR0101T	1.0	0.2	B
185	396	0036+4803	0 38 57.23	48 20 15.2	−227	144	120	11.00	−5	dE3 pec	S	15/03/93	X1AR0701T	1.5	0.4	SW
224[a]	454	0040+4100	0 42 44.20	41 16 7.7	−297	2000	802	4.30	3	Sb I-II	A	21/07/91	X0MC5101T	10.2	2.2	FS
404	718	0106+3527	1 9 27.00	35 43 4.5	−36	60	60	11.30	−3	$S0_3$	L	19/06/93	X1AR0C01T	3.5	0.2	P
628	1149	0134+1531	1 36 41.67	15 47 2.5	659	120	120	10.50	5	Sc I	A	07/07/93	X1AR0K01T	1.7	0.4	SW
672	1256	0145+2711	1 47 53.95	27 25 55.9	411	72	28	11.40	6	SBc III	H	26/06/93	X1AR0N01T	3.2	0.4	SW
...	2082	0233+2512	2 36 16.23	25 25 23.8	710	63	11	14.00	6	...	...	18/07/93	X1AR0T01T	0.9	0.3	B
1023	2154	0237+3850	2 40 23.88	39 3 47.8	648	85	40	10.50	−3	$SB0_1$	A	19/03/93	X1AR0W01T	4.0	1.1	F
1560	3060	0427+7146	4 32 48.94	71 52 59.0	−28	100	18	12.10	7	...	H	22/03/93	X1AR1W01T	1.5	0.4	B
2768	4821	0907+6014	9 11 40.39	60 1 57.6	1363	65	30	11.10	−5	$S0_{1/2}$	L	30/04/93	X1AR2R01T	1.2	0.4	B
2903	5079	0929+2143	9 32 10.05	21 30 2.0	539	133	60	9.80	4	Sc I-II	H	19/03/93	X1AR2W01T	29.2	2.4	S
3079	5387	0958+5555	10 1 58.40	55 40 51.2	1114	87	16	11.20	5	...	S	30/04/93	X1AR3001T	2.9	1.0	W
3077	5398	0959+6858	10 3 19.18	68 43 59.3	7	60	45	10.70	0	...	H	22/03/93	X1AR3101T	21.9	5.0	S
3198	5572	1016+4548	10 19 54.89	45 32 59.5	660	100	38	10.70	5	Sc I-II	H	24/04/93	X1AR3601T	1.2	0.3	W
3319	5789	1036+4156	10 39 9.37	41 41 13.9	743	75	43	12.00	6	SBc II.4	H:	15/03/93	X1AR3B01T	3.8	0.7	FPS
3344	5840	1040+2511	10 43 31.08	24 55 20.5	698	75	70	11.10	4	Sbc I.2	H:	22/04/93	X1AR3D01T	6.1	0.8	P
3359	5873	1043+6329	10 46 36.76	63 13 28.1	1013	80	48	11.00	5	SBc I.8	H	23/03/93	X1AR3F01T	7.0	1.3	S
3368	5882	1044+1205	10 46 45.59	11 49 17.7	899	75	50	10.00	2	Sab II	L	10/05/93	X1AR3G01T	1.9	0.2	P
3432	5986	1049+3653	10 52 31.11	36 37 9.5	611	75	20	11.70	9	Scd	H	27/04/93	X1AR3H01T	8.7	1.6	S
3486	6079	1057+2914	11 0 23.89	28 58 30.3	679	72	51	11.20	5	Sbc I.2	S	22/04/93	X1AR3I01T	2.9	0.5	PS
3521	6150	1103+0014	11 5 49.26	0 2 2.3	804	135	70	10.10	4	Sbc II	S:	08/05/93	X1AR3L01T	4.0	0.3	FS
3627	6346	1117+1315	11 20 15.07	12 59 21.7	737	90	42	8.90	3	Sb II.2	T	08/07/93	X1AR3Q01T	1.7	0.2	FW
3718	6524	1129+5320	11 32 35.05	53 4 5.2	987	110	50	11.80	1	S pec?	L	30/04/93	X1AR3X01T	1.9	0.7	B
3953	6870	1151+5236	11 53 48.91	52 19 35.4	1037	65	34	10.80	4	SBbc I-II	T	12/07/93	X1AR4101T	1.6	0.3	FW
4145	7154	1207+4009	12 10 1.62	39 52 58.7	1013	65	43	12.20	7	Sc II	T	15/04/93	X1AR4801T	2.1	0.7	S
4151[a]	7166	1208+3941	12 10 31.50	39 24 12.8	970	70	60	11.20	2	Sab	S	10/07/95	X2PJ0103P	126.0	13.0	FP
4157	7183	1208+5045	12 11 5.00	50 29 7.6	771	77	13	11.90	3	Sbc	H	01/05/93	X1AR4901T	1.4	0.2	B
4192	7231	1211+1510	12 13 48.24	14 54 1.0	−98	99	22	11.00	2	Sb II	T	15/05/93	X1AR4A01T	1.4	0.2	W
4214[a]	7278	1213+3637	12 15 39.00	36 19 50.0	288	110	90	10.30	10	SBm III	H	04/03/93	X1A80E01T	54.4	3.5	PS
4216	7284	1213+1325	12 15 54.25	13 8 59.2	135	85	17	11.20	3	Sb	T	15/05/93	X1AR4C01T	1.4	0.3	B
4244	7322	1215+3805	12 17 29.46	37 48 23.9	247	185	23	10.80	6	Scd	H	19/06/93	X1AR4E01T	2.6	0.3	S

TABLE 2.—*Continued*

NGC (1)	UGC (2)	Pos. 1950 (3)	R.A.(J2000) (4)	Dec.(J2000) (5)	V_h (6)	D_a (7)	D_b (8)	B_{mag} (9)	T (10)	Classif. (11)	Sp. (12)	Date (13)	Rootname (14)	f_{UV} (15)	σ (16)	Morph. (17)
4438	7574	1225+1317	12 27 45.62	13 0 32.2	86	97	39	12.00	0	Sb	L	16/07/93	X1AR4K01T	1.5	0.3	W
4486[a]	7654	1228+1240	12 30 49.80	12 23 28.3	1292	70	70	10.40	−6	E0	L	05/04/91	X0IF0201T	1.6	0.2	P
4527	7721	1231+0255	12 34 8.47	2 39 11.5	1730	65	22	12.40	4	Sb II	T	15/03/93	X1AR4Q01T	1.5	0.4	B
4565	7772	1233+2615	12 36 20.67	25 59 15.0	1227	155	19	10.30	3	Sb	S	12/07/93	X1AR401T	1.3	0.3	W
4569	7786	1234+1326	12 36 49.96	13 9 44.6	−223	114	47	11.80	2	Sab I-II	L	30/06/93	X1AR4V01T	9.7	0.6	P
4579	7796	1235+1205	12 37 43.53	11 49 5.9	1502	60	50	11.50	3	Sab II	L	19/05/93	X1AR4W01T	3.4	0.5	P
4605	7831	1237+6153	12 40 0.06	61 36 31.1	150	70	25	10.80	5	Sc III	H	12/07/93	X1AR4X01T	4.7	2.3	S
4636	7878	1240+0257	12 42 49.70	2 41 18.4	937	70	50	11.80	−5	$E/S0_1$	L	10/05/93	X1AR4Z01T	1.8	0.3	F
4649	7898	1241+1149	12 43 39.84	11 33 11.0	1095	70	60	10.30	−5	$S0_1$	A	12/07/93	X1AR5001T	4.5	0.4	F
4656	7907	1241+3226	12 43 58.46	32 10 20.2	649	220	30	10.60	9	Im	H	02/05/93	X1AR5101T	16.2	2.9	S
4725	7989	1248+2546	12 50 26.38	25 30 3.2	1207	120	90	10.20	2	Sb/SBb II	S	22/05/93	X1AR5301T	1.8	0.2	F
4736	7996	1248+4123	12 50 53.05	41 7 12.7	307	140	120	8.70	2	RSab	L	18/07/93	X1AR5401T	12.6	1.8	FP
4762	8016	1250+1130	12 52 55.93	11 13 50.3	1006	90	20	11.10	−2	$S0_1$	L	20/05/93	X1AR5501M	2.0	0.4	FW
4866	8102	1256+1426	12 59 27.18	14 10 16.0	1980	60	13	11.90	−1	Sa	L	05/05/93	X1AR5701T	1.2	0.2	FW
...	8188	1303+3752	13 5 49.18	37 36 24.2	326	70	60	14.00	9	...	...	30/04/93	X1AR5A01T	1.2	0.1	SW
5005	8256	1308+3719	13 10 56.62	37 3 32.1	1022	63	30	10.60	4	Sb II	T	31/05/93	X1AR5C01T	3.5	0.4	S
5023	8286	1310+4418	13 12 11.88	44 2 20.4	400	75	8	13.20	−5	...	...	28/04/93	X1AR5D01T	2.2	0.4	S
5055	8334	1313+4217	13 15 49.25	42 1 49.3	497	150	90	9.70	4	Sbc II-III	T	26/04/93	X1AR5F01T	3.8	0.6	PS
5194[a]	8493	1327+4727	13 29 51.90	47 11 50.3	474	90	75	8.80	4	Sbc I-II	S	23/03/93	X14X0401T	3.4	0.3	FS
5195	8494	1327+4731	13 29 59.24	47 15 59.5	558	70	50	10.60	0	$SB0_1$ pec.	L:	01/05/93	X1AR5L01T	1.5	0.4	W
5248	8616	1335+0908	13 37 32.06	8 53 6.9	1156	68	50	11.40	4	Sbc I-II	H	19/07/93	X1AR5N01T	8.5	1.7	R
5322	8745	1347+6026	13 49 15.19	60 11 26.2	1804	60	40	11.30	−5	E4	L:	26/04/93	X1AR5Q01T	3.2	0.8	FW
5364	8853	1353+0515	13 56 11.99	5 0 53.0	1330	72	55	13.20	4	Sc I	H	01/06/93	X1AR5S01T	1.2	0.3	W
5474	9013	1403+5354	14 5 1.32	53 39 44.3	277	65	53	11.90	6	Scd IV	H	24/04/93	X1AR5T01T	4.4	0.8	S
5566	9175	1417+0409	14 20 19.92	3 56 1.4	1569	62	23	12.00	2	SBa II	L	01/06/93	X1AR5Y01T	2.3	0.2	F
5866	9723	1505+5557	15 6 29.41	55 45 49.3	672	65	30	11.10	−1	$S0_3$	T	22/05/93	X1AR6301T	1.5	0.4	W
5907	9801	1514+5630	15 15 53.41	56 19 44.6	666	128	18	11.40	5	Sc	H:	25/04/93	X1AR6501T	1.4	0.2	W
6015	10075	1550+6227	15 51 25.34	62 18 34.0	834	70	24	11.70	6	Sc II-III	H	31/05/93	X1AR6701T	1.2	0.5	SW
6503	11012	1749+7009	17 49 27.16	70 8 42.7	60	80	26	10.90	6	Sc II.8	T:	11/07/93	X1AR6E01T	2.9	0.5	S
6946	11597	2033+5959	20 34 52.46	60 9 13.5	48	140	140	10.50	6	Sc II	H	24/06/93	X1AR6K01T	1.1	0.3	B
7331	12113	2234+3409	22 37 4.07	34 24 58.4	819	114	40	10.40	4	Sb I-II	T	16/07/93	X1AR6R01T	1.5	0.1	FSW

NOTES TO TABLE 2.—See § 3.1 for explanations of Table entries. Footnote "a" next to the galaxy NGC number denotes archival images, generally obtained with a different FOC format, filter, or exposure time than those of the program galaxies; see § 3.3 for details.

with a 5% absolute calibration uncertainty (Meurer 1995) to produce the quoted flux uncertainty. Except for bright and concentrated sources, the flux uncertainty is dominated by the uncertainty in the background determination. The cause of artificial background variations across the image is imperfect flat-fielding. Furthermore, a systematic error in background determination is unavoidable due to the small field of view which covers only a fraction of the optical extent of these galaxies. Some of this systematic error is accounted for by the above procedure for estimating the background uncertainty. Nevertheless, the total UV fluxes quoted here agree well with the 2300 Å fluxes measured for those galaxies that have also been observed with *IUE* (Kinney et al. 1993; see also Meurer 1995), which has a comparable entrance aperture. This suggests that the regions of the images with the lowest counts are, in fact, devoid of significant UV emission. The UV fluxes given here should be used with care and in conjunction with the UV-morphology classification (col. 17) and the visual appearance of the image. For example, there is low significance to the flux that is listed for a galaxy which appears blank. The UV fluxes are uncorrected for Milky Way or external extinction.

Column (17): UV morphologies roughly describing the *HST* image, with the following symbols: B, blank image; W, weak or nearly absent UV emission; S, star-forming morphology, with knots and compact sources of UV emission; F, diffuse, centrally concentrated emission; P, unresolved nuclear point-source; R, circumnuclear star-forming ring. Some comments on each of these types follow.

We have rechecked the coordinates and pointing of the blank (B morphology) images and verified that they are not cases of telescope mispointing. As a check on the pointing accuracy, there are about 40 images which display a feature that can be securely associated with the nucleus of the galaxy. In almost all cases it is within 3″ of the center of the image, as expected from the combined uncertainty in the GASP coordinates of the nucleus and the *HST* pointing accuracy. In the few cases where the nucleus is further from the image center, this has been traced to inaccurate input coordinates (see § 3.3). The blank images are also not the result of foreground Milky Way extinction, except for two galaxies, NGC 1560 and NGC 6946, which lie near the Galactic plane. Dust in the disks of the galaxies themselves is probably a factor, since 10 out of 13 galaxies with B morphologies have minor-to-major axis ratios less than 0.5 (i.e., an inclination greater than 60°). The fact that the centers of many galaxies are weak UV emitters is confirmed by the detection of very weak (W-type) but significant and centrally concentrated emission in many of the galaxies, which establishes that the galactic nucleus is, indeed, in the field of view.

The compact sources seen in the S-type morphologies are probably compact young star clusters, or in some cases individual O and B stars. Similar objects have been detected with *HST* in a variety of starburst environments (e.g., Meurer et al. 1995; Maoz et al. 1996). They will be studied in further detail by Ho et al. (1996b).

The diffuse F-type emission occurs in some of the early-type spirals and the ellipticals in the sample. We believe that, in general, this observed feature is dominated by actual UV emission from an evolved spheroidal stellar population (the "UV upturn"; see, e.g., Burstein et al. 1988), rather than visual-band emission leaking through the F220W filter, based on several tests described in § 2. In individual cases, however, confirmation by means of blue and near-UV imaging photometry of the center of each of these galaxies is required.

Galaxies with bright nuclear UV point sources (P-type) have been discussed in detail by Maoz et al. (1995), especially in the context of low-luminosity AGNs. They showed that ~20% of the northern LINER galaxies display a nuclear point source in the FOC images, with a UV flux that, if extrapolated beyond the Lyman limit, could be sufficient to produce the observed strength of optical emission lines through photoionization. While this was the first direct detection of what may be the AGN-like ionizing source in LINER galaxies, it raised the question of why such a source is *not* detected in 80% of LINERs. Several of the P-type sources in this paper, especially the weak ones and those in archival images, were not included in Maoz et al. (1995). However, the fraction of "UV-bright" LINERs, or LINERs plus Seyferts, remains unchanged. For example, among the 35 northern galaxies with spectral classification T, L, or S (transition-type, LINER, or Seyfert), nine have a nuclear UV point source.

The five circumnuclear rings in the sample (designated "R") have been discussed in detail by Maoz et al. (1996), who show that a large, possibly dominant fraction of the UV light in these objects is emitted by the numerous compact sources distributed along the rings. These sources are probably young and massive star clusters that will remain bound, similar to those seen with *HST* in other starburst environments.

3.2. *Pictorial Atlas*

Figures 1 (Plates 29–36) and 2 (Plates 37–47) are gray-scale representations of the FOC images of the southern and northern galaxies, respectively. Each of the six frames on each page has a scale of 22″ × 22″ and has been rotated so that north is up and east is to the left. Archival exposures are marked with an asterisk next to the galaxy name, and in some cases have a different field of view and sensitivity; see § 3.3 for details. The gray scale of each image is chosen to bring out the most interesting details. However, these snapshots cannot convey all of the useful information in many of the images, and the reader is advised to refer to § 3.3 or to retrieve the actual data from the *HST* archive, if complete details are required. This is true both for bright sources, where a single gray scale cannot show details of different contrast, and for weak sources (W-type morphology), where the faint emission is lost in the reproduction.

3.3. *Notes on Individual Objects*

3.3.1. *Southern Galaxies*

NGC 247 (0044−2102).—This late-type galaxy has a bright UV point source at a position consistent with the optical nucleus of the galaxy, which has an H II-like spectrum (Maoz et al. 1995). In addition, there are numerous compact sources in the image. See Maoz et al. (1995) for further details.

NGC 300 (0052−3757).—There are about a dozen compact sources in the UV image, the brightest of which is resolved (FWHM ≈ 0.″2) and is probably at the nucleus of this face-on Sd galaxy. The second brightest source, 3″ to the east, is unresolved (FWHM < 0.″1).

NGC 1079 (0241−2912).—The small (4″ diameter) circumnuclear star-forming ring seen in the *HST* image of this

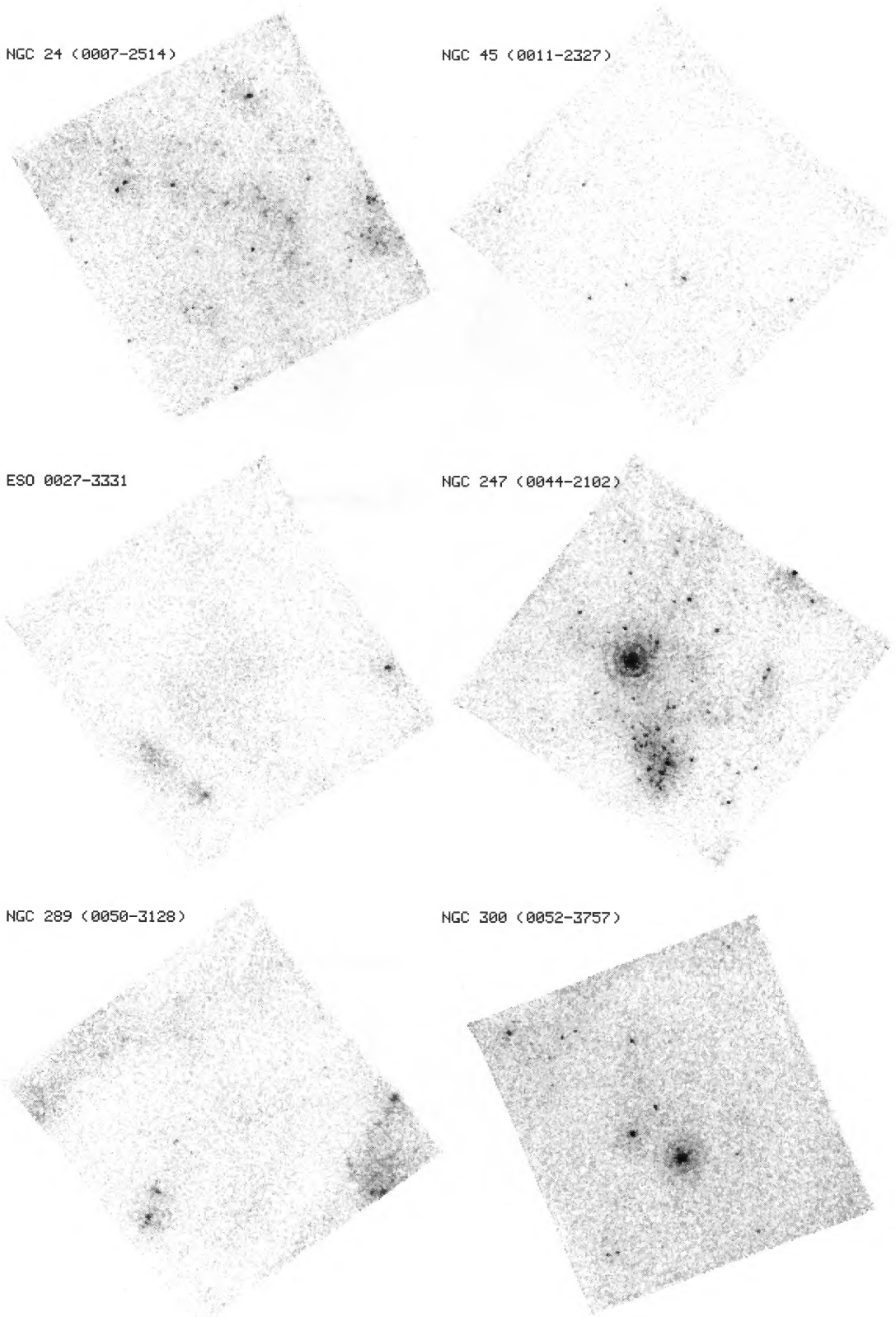

FIG. 1.—Gray-scale representations of the FOC images of the southern galaxies. Each of the six frames on each page has a scale of 22″ × 22″ and has been rotated so that north is up and east is to the left. Archival exposures are marked with an asterisk next to the galaxy name and in some cases have a different field of view and sensitivity; see § 3.3 for details. The gray scale of each image is chosen to bring out the most interesting details. However, these snapshots cannot convey all of the useful information in many of the images, and the reader is advised to refer to § 3.3, or to retrieve the actual data from the *HST* archive, if complete details are required.

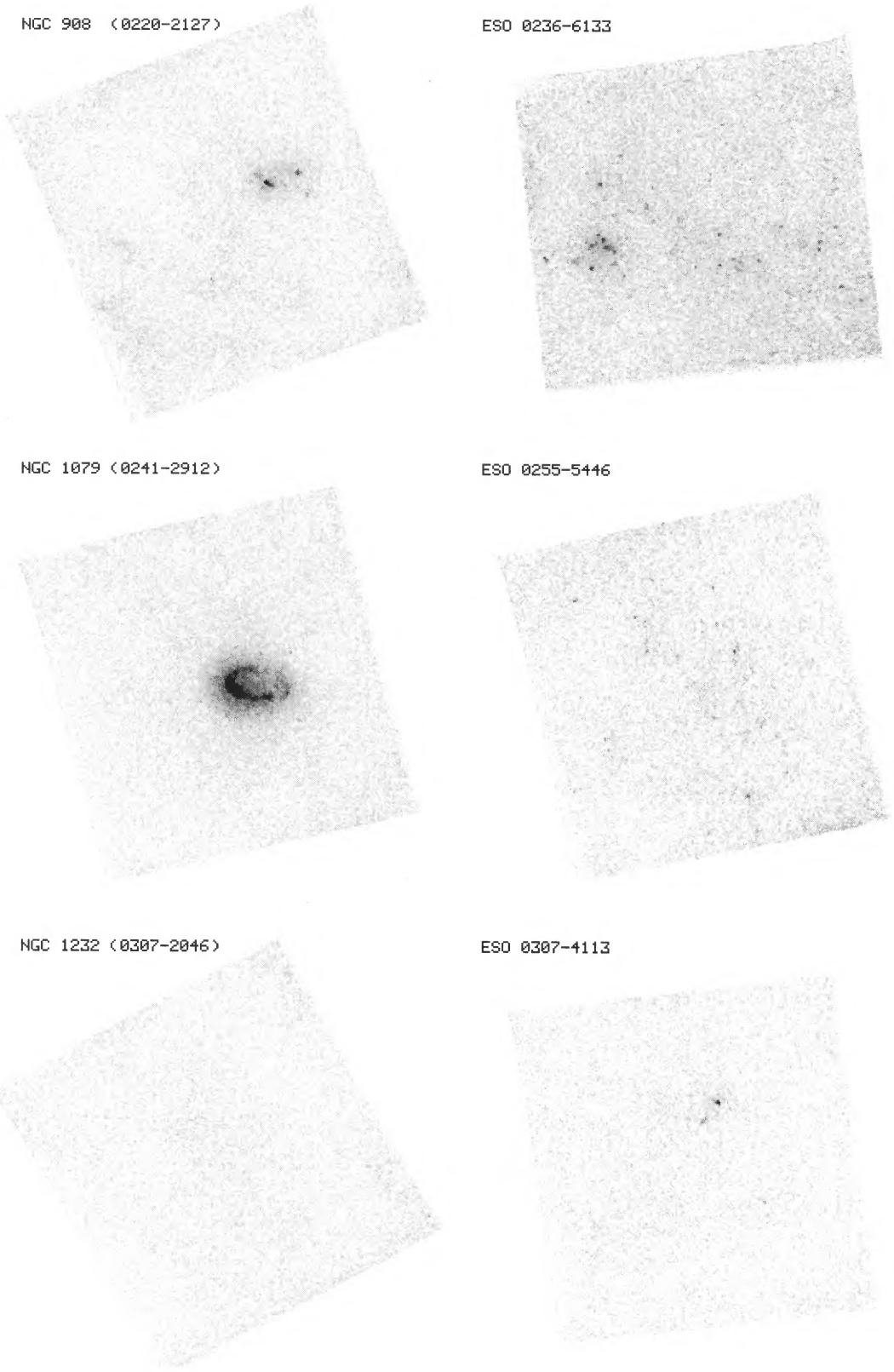

FIG. 1.—*Continued*

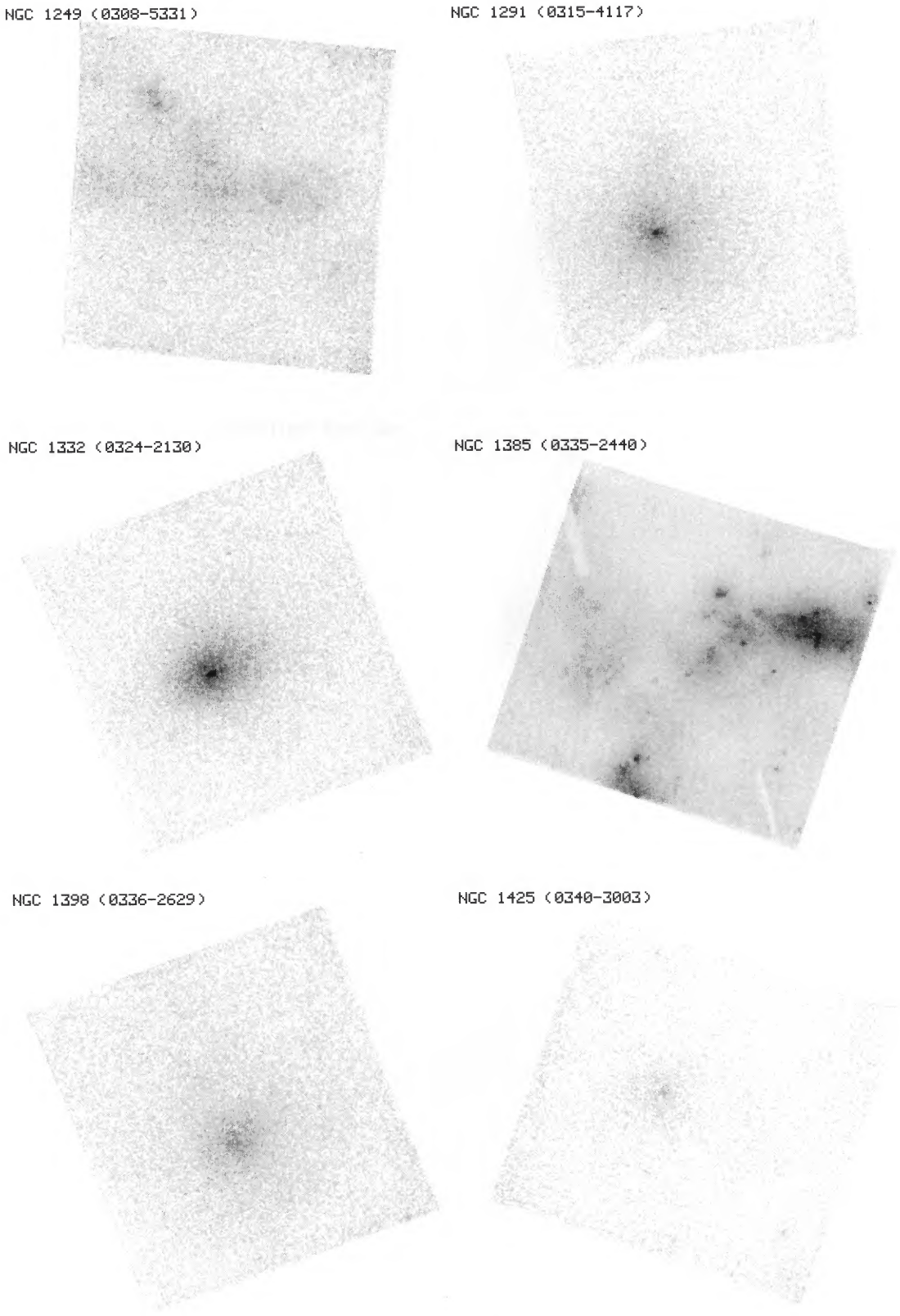

FIG. 1.—*Continued*

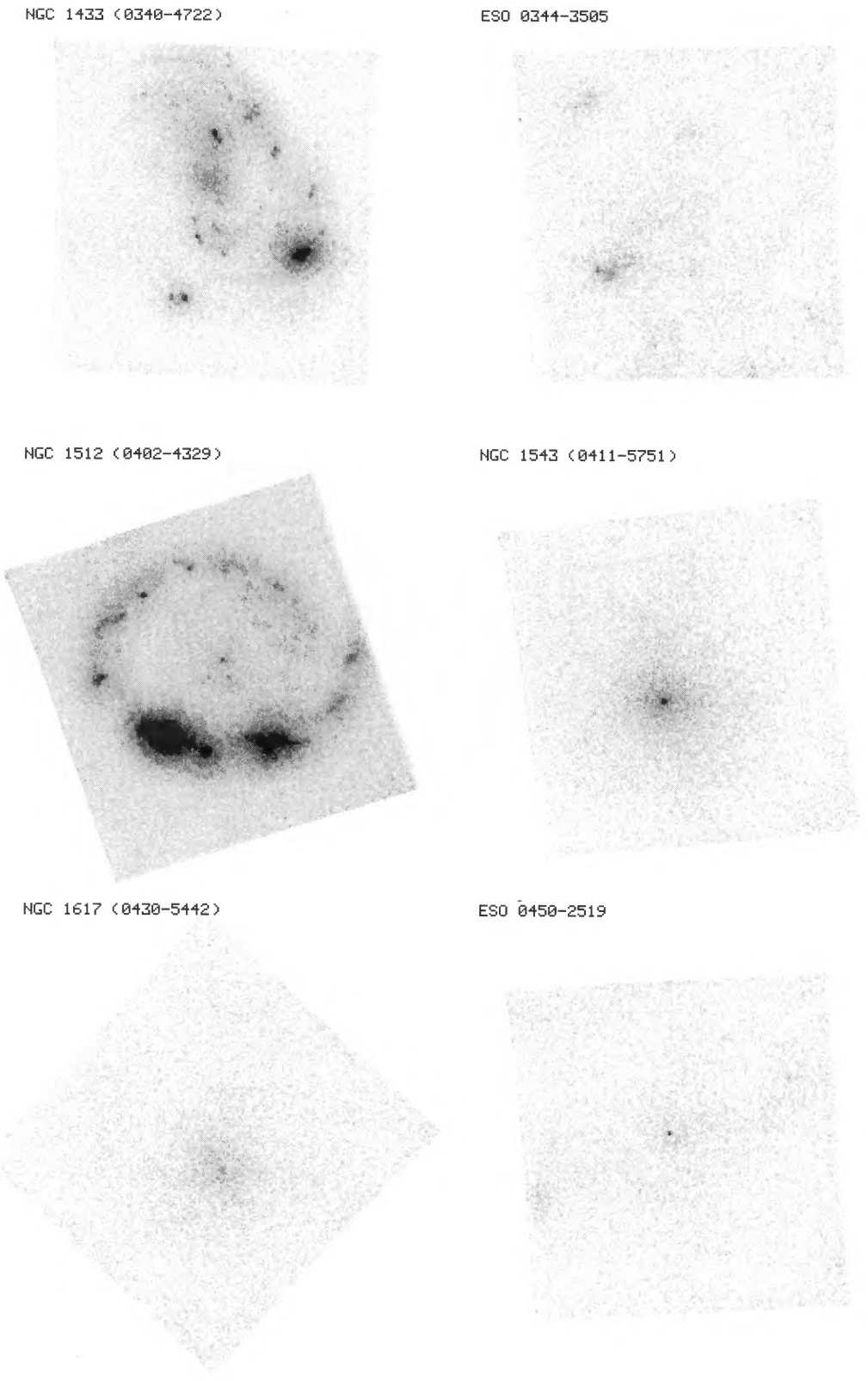

FIG. 1.—*Continued*

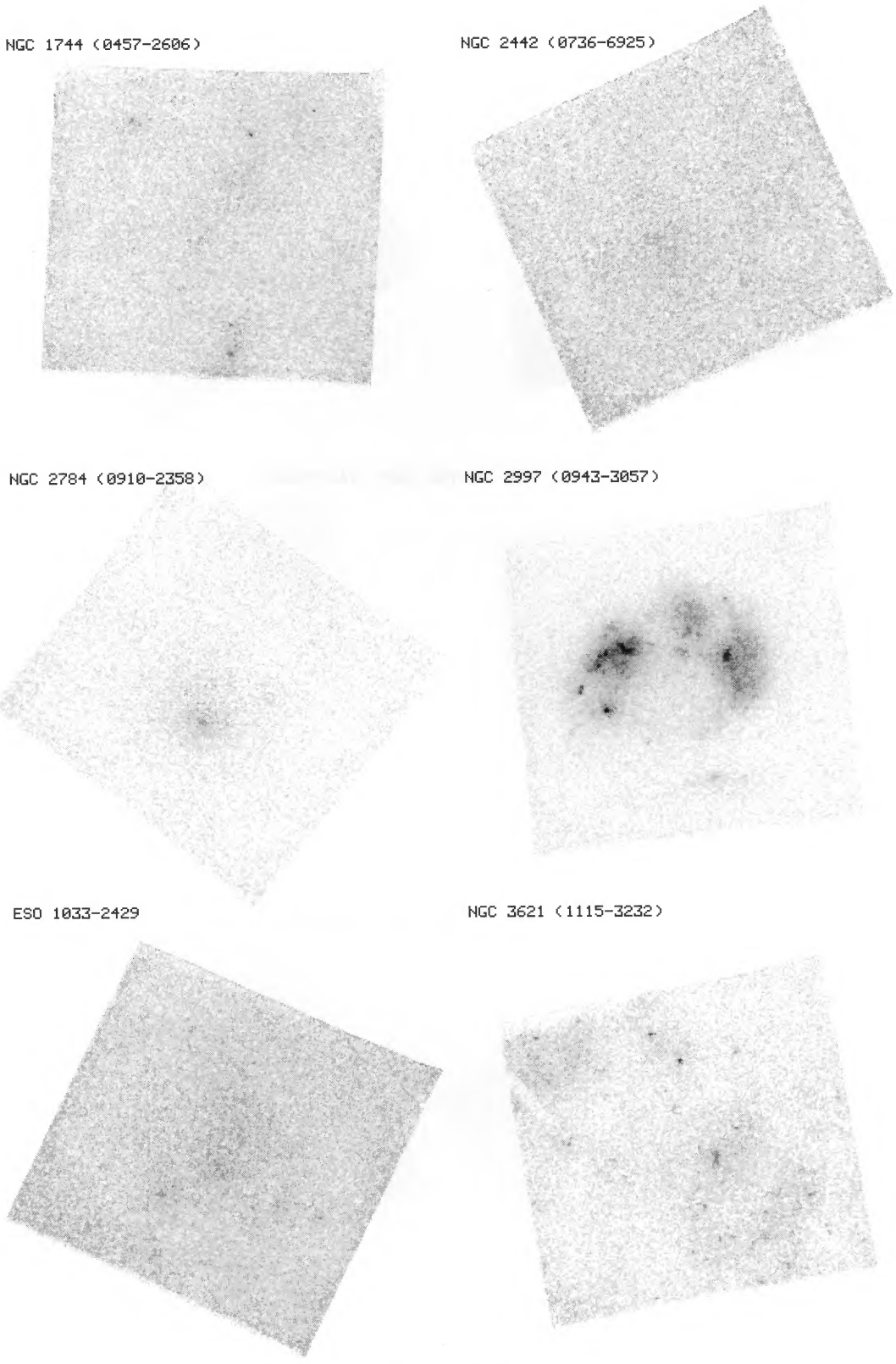

FIG. 1.—*Continued*

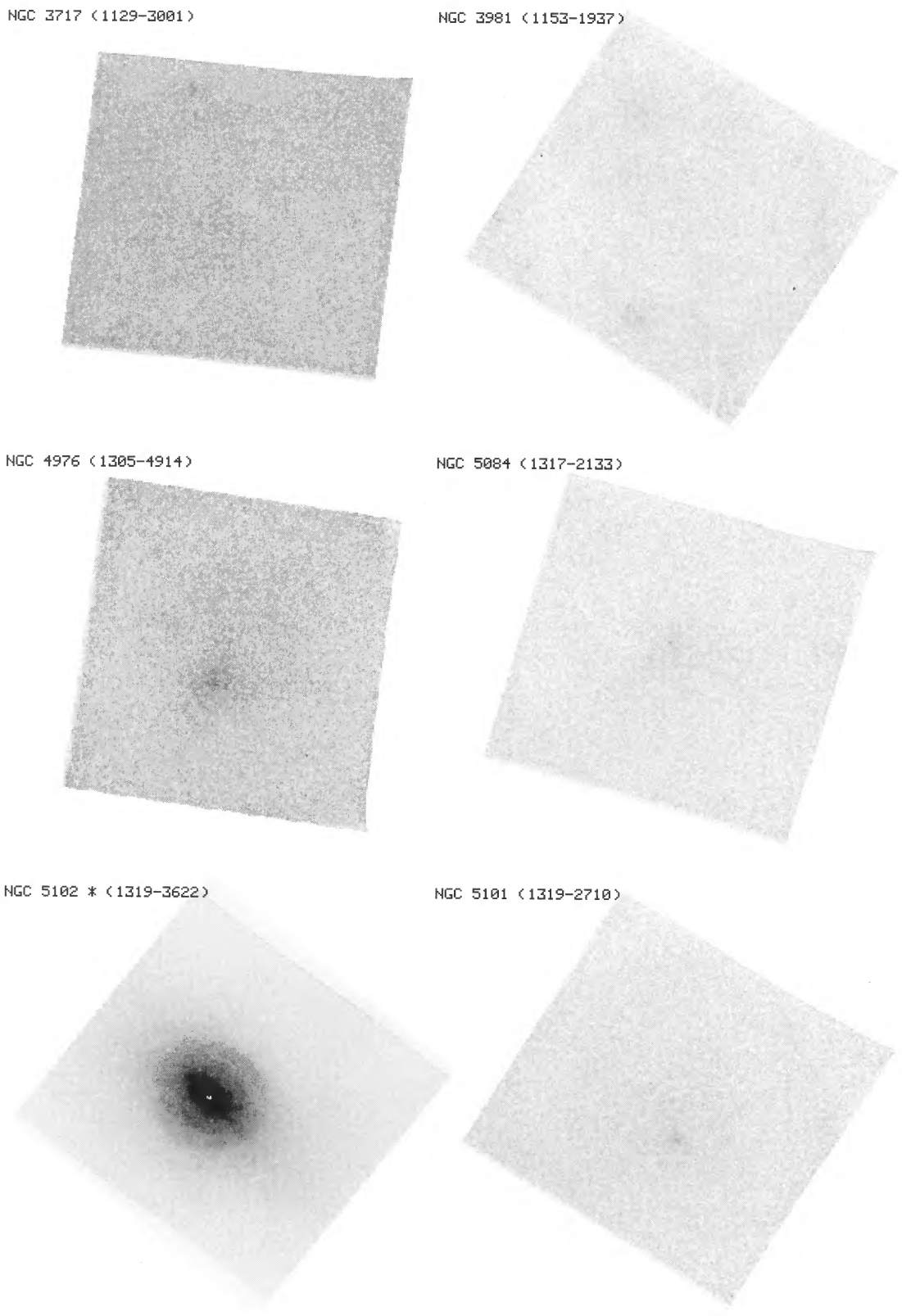

FIG. 1.—*Continued*

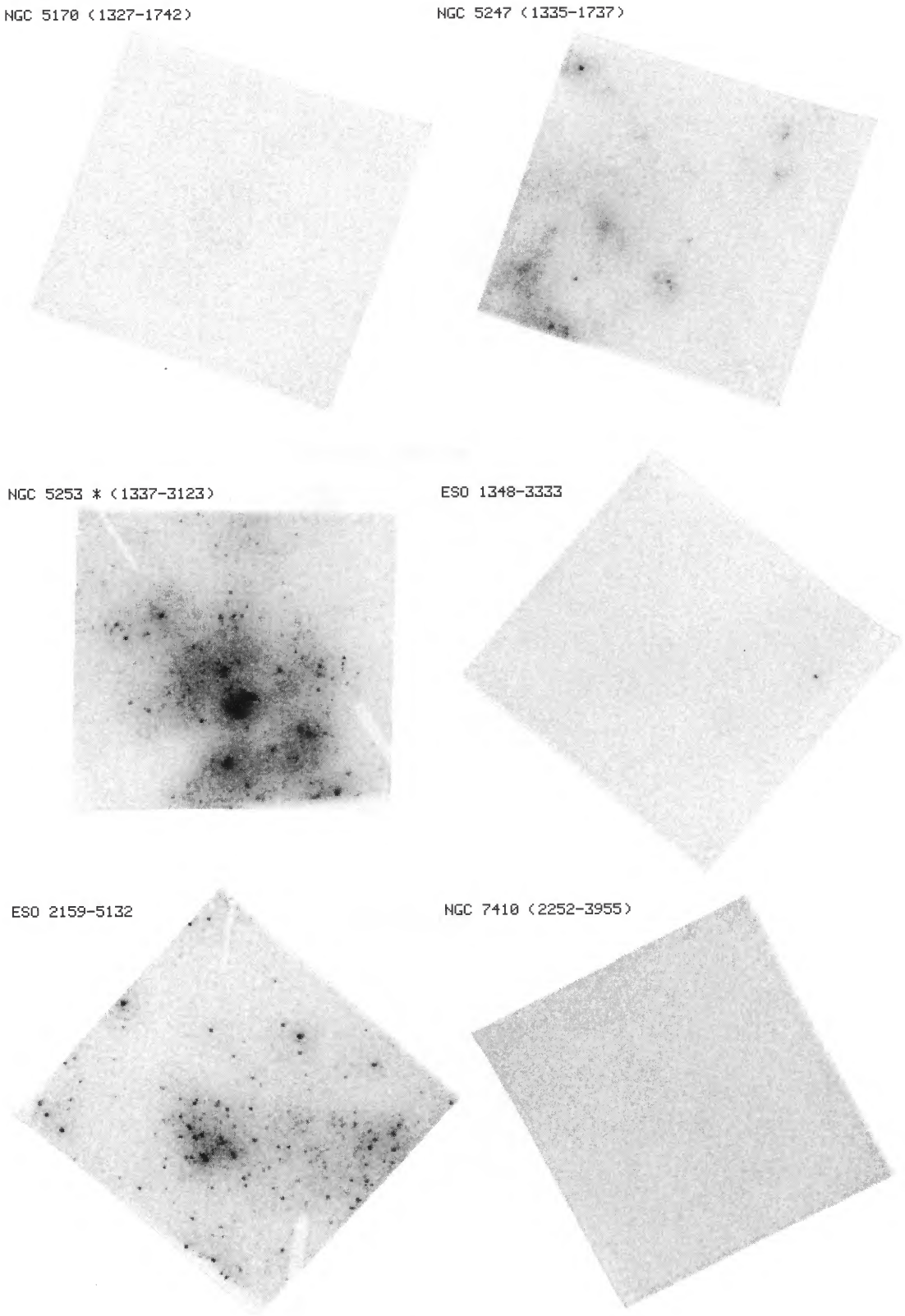

FIG. 1.—*Continued*

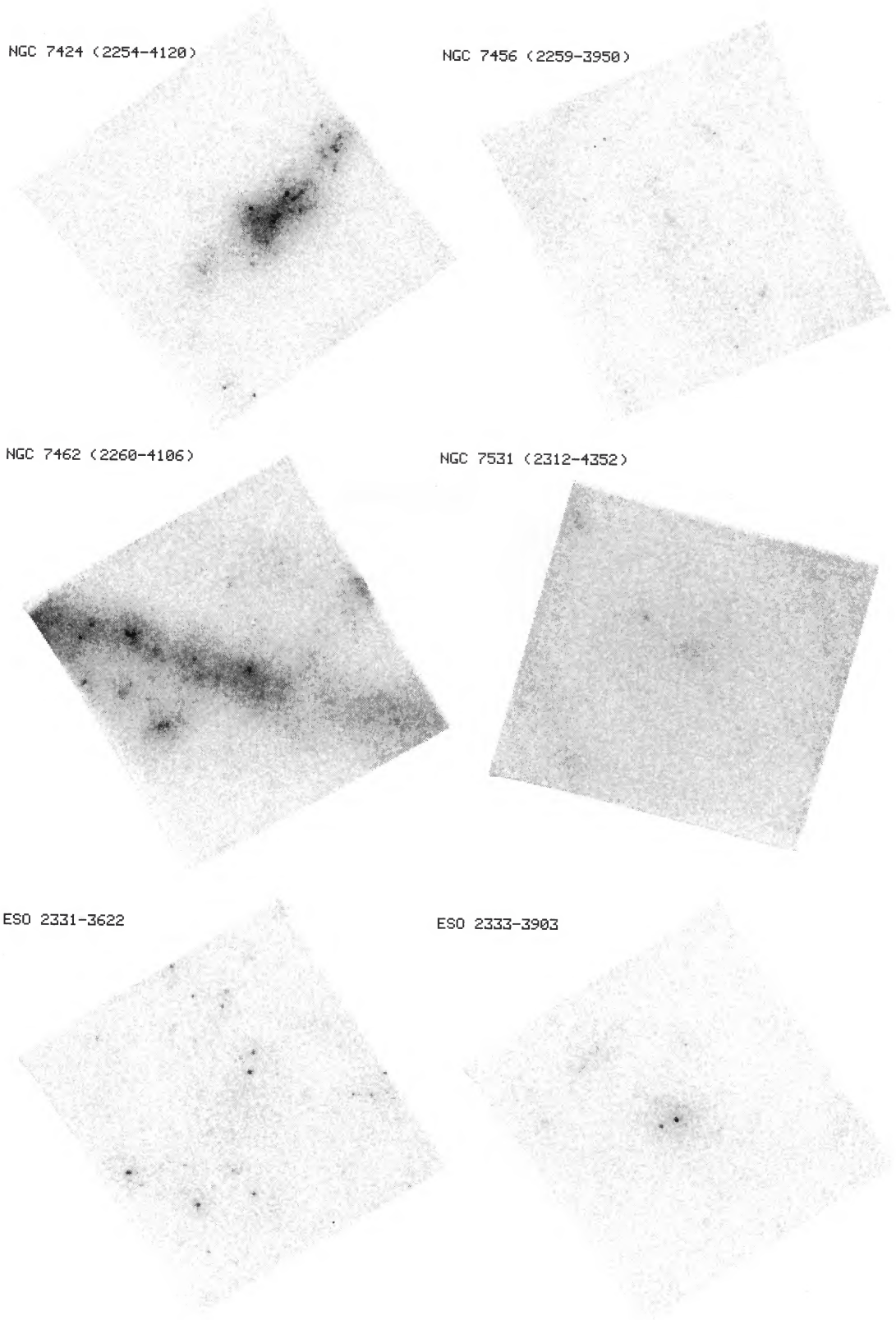

FIG. 1.—*Continued*

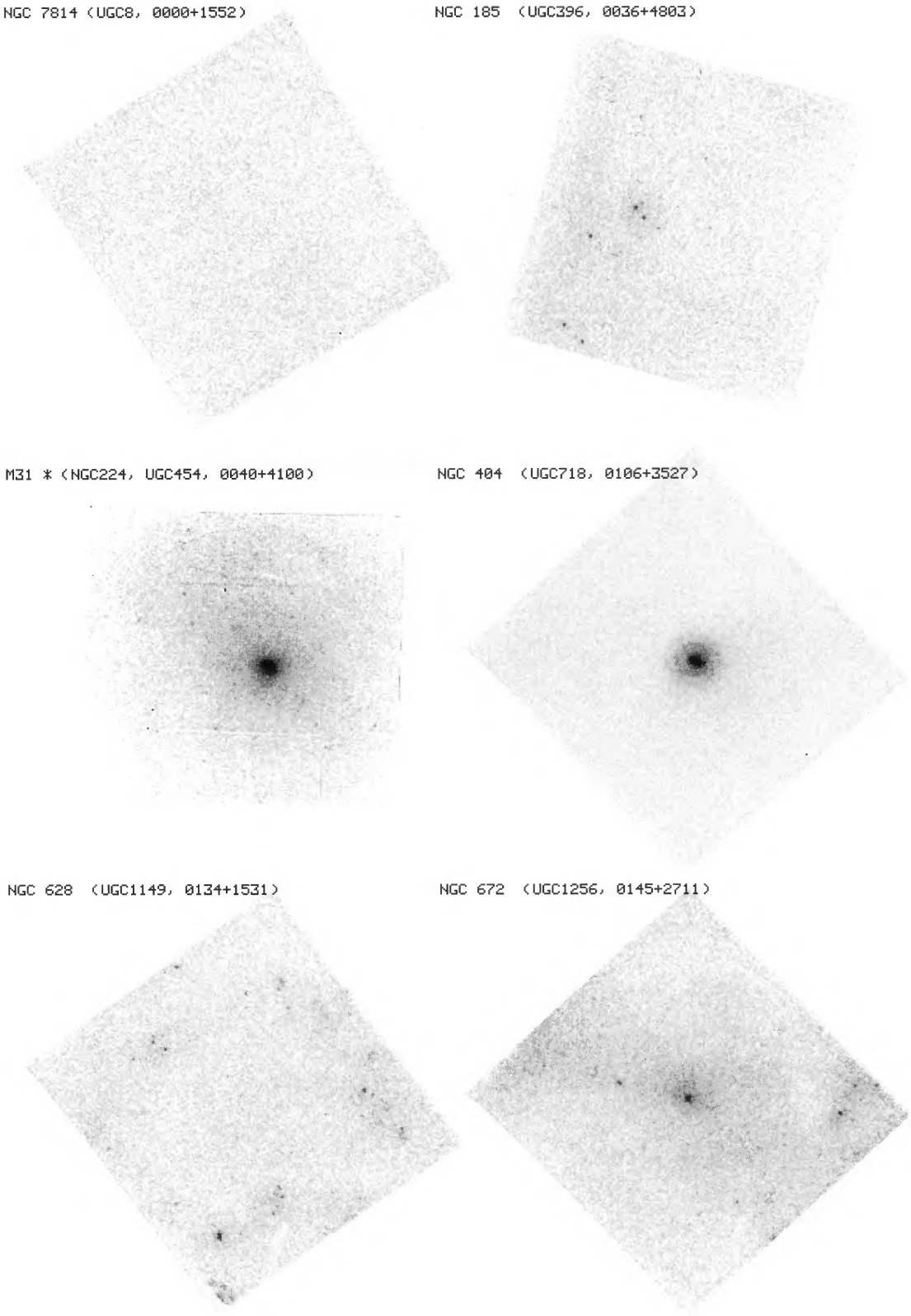

FIG. 2.—Same as Fig. 1, but for the northern galaxies

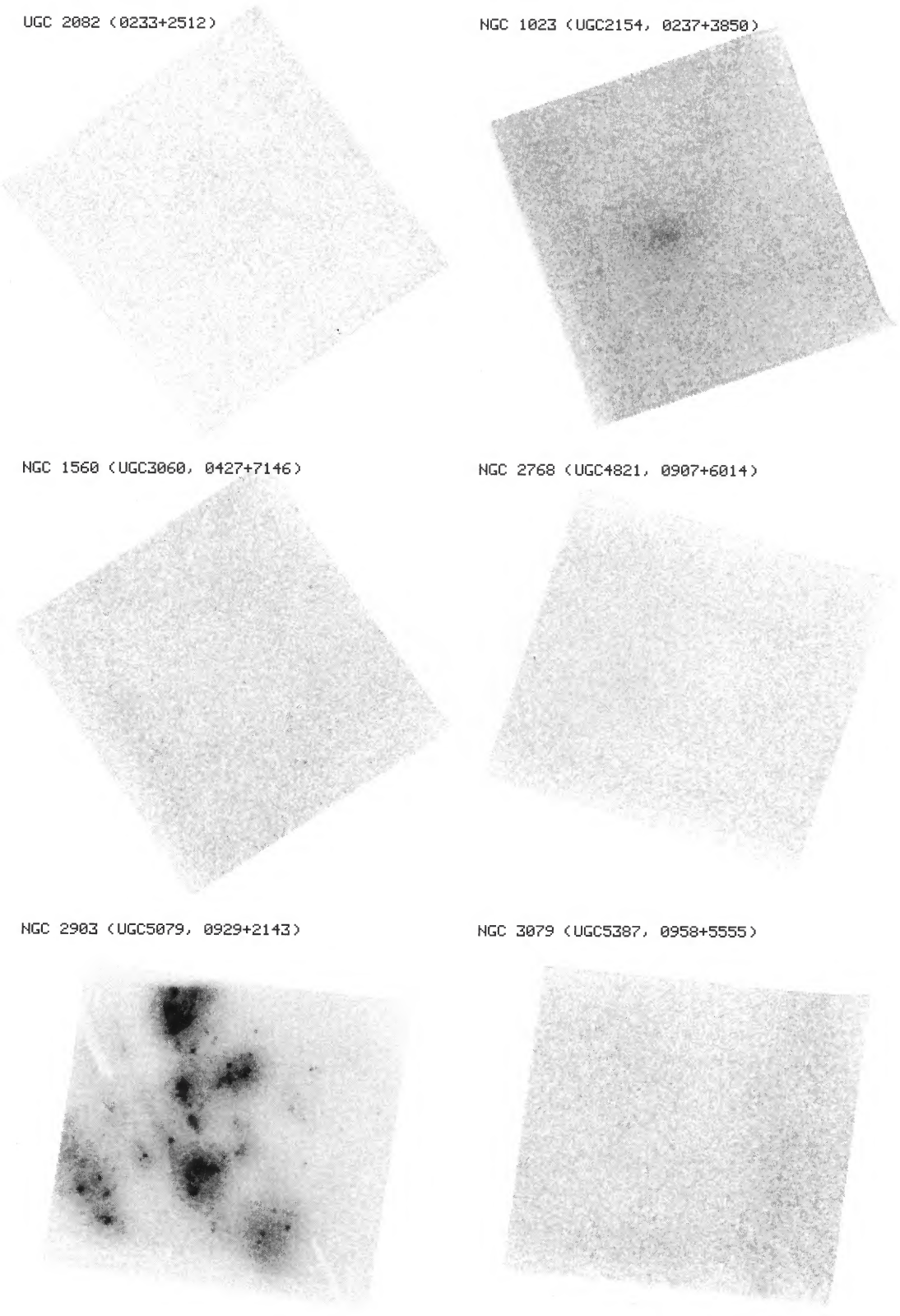

FIG. 2.—*Continued*

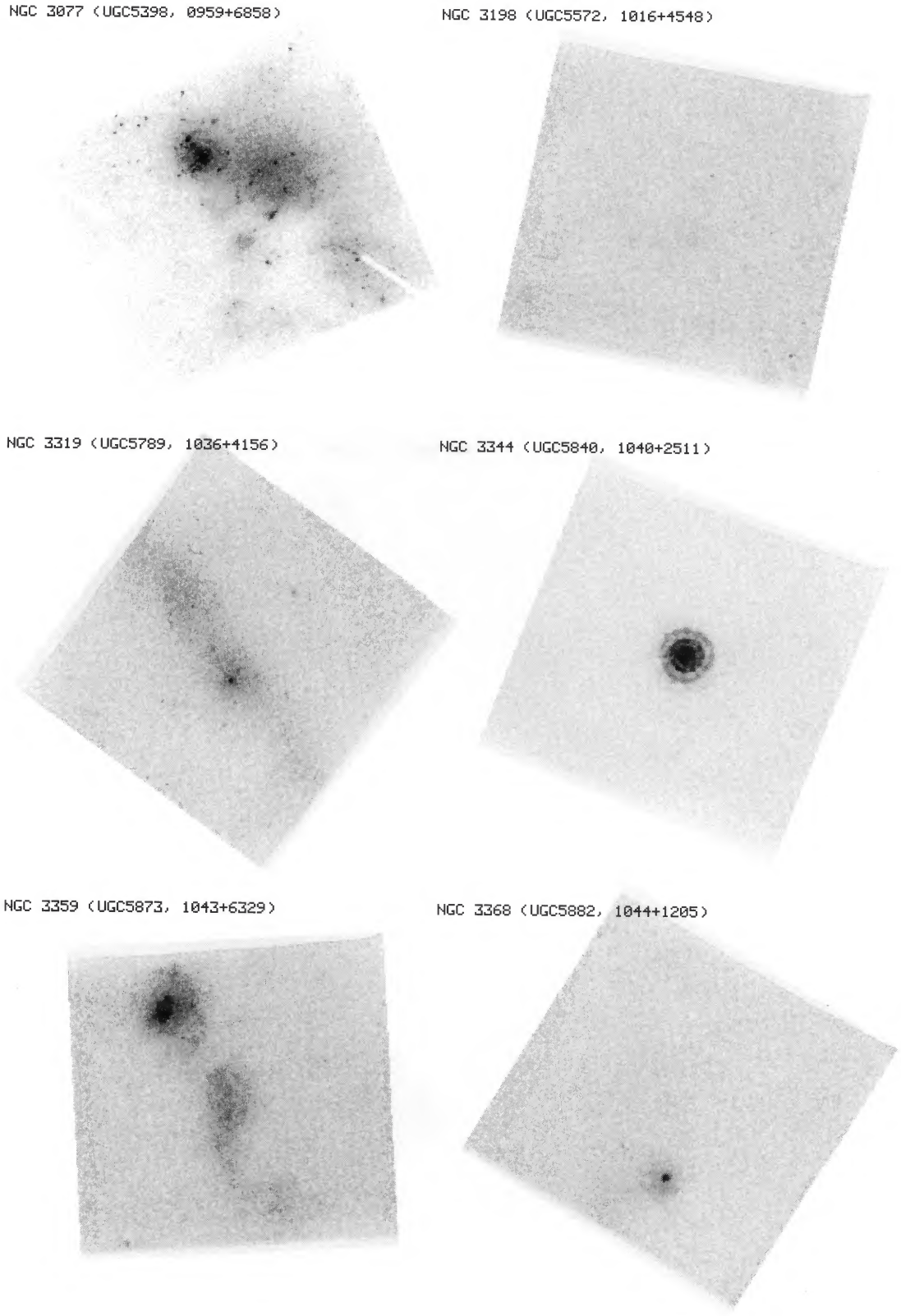

FIG. 2.—*Continued*

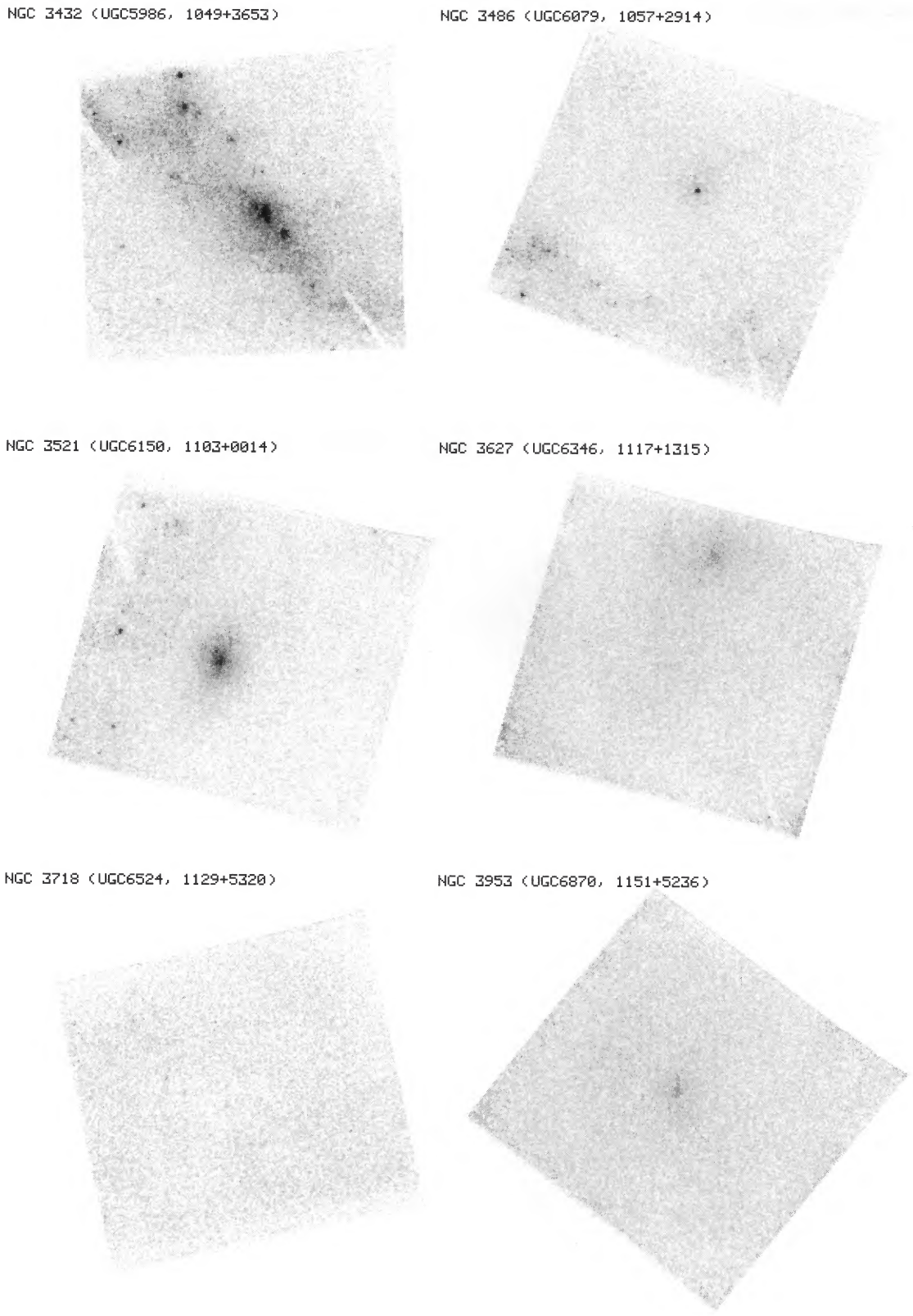

FIG. 2.—*Continued*

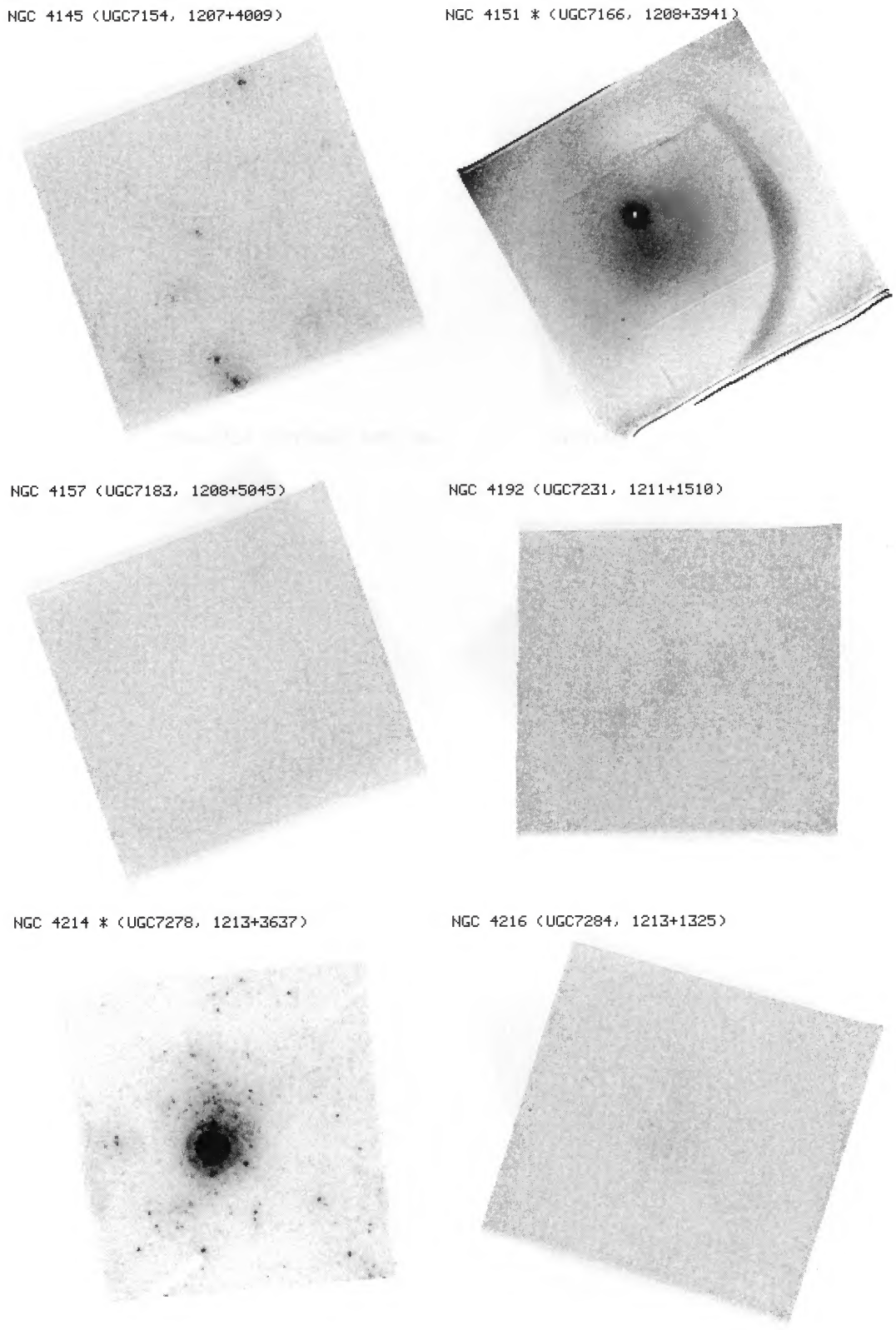

FIG. 2.—*Continued*

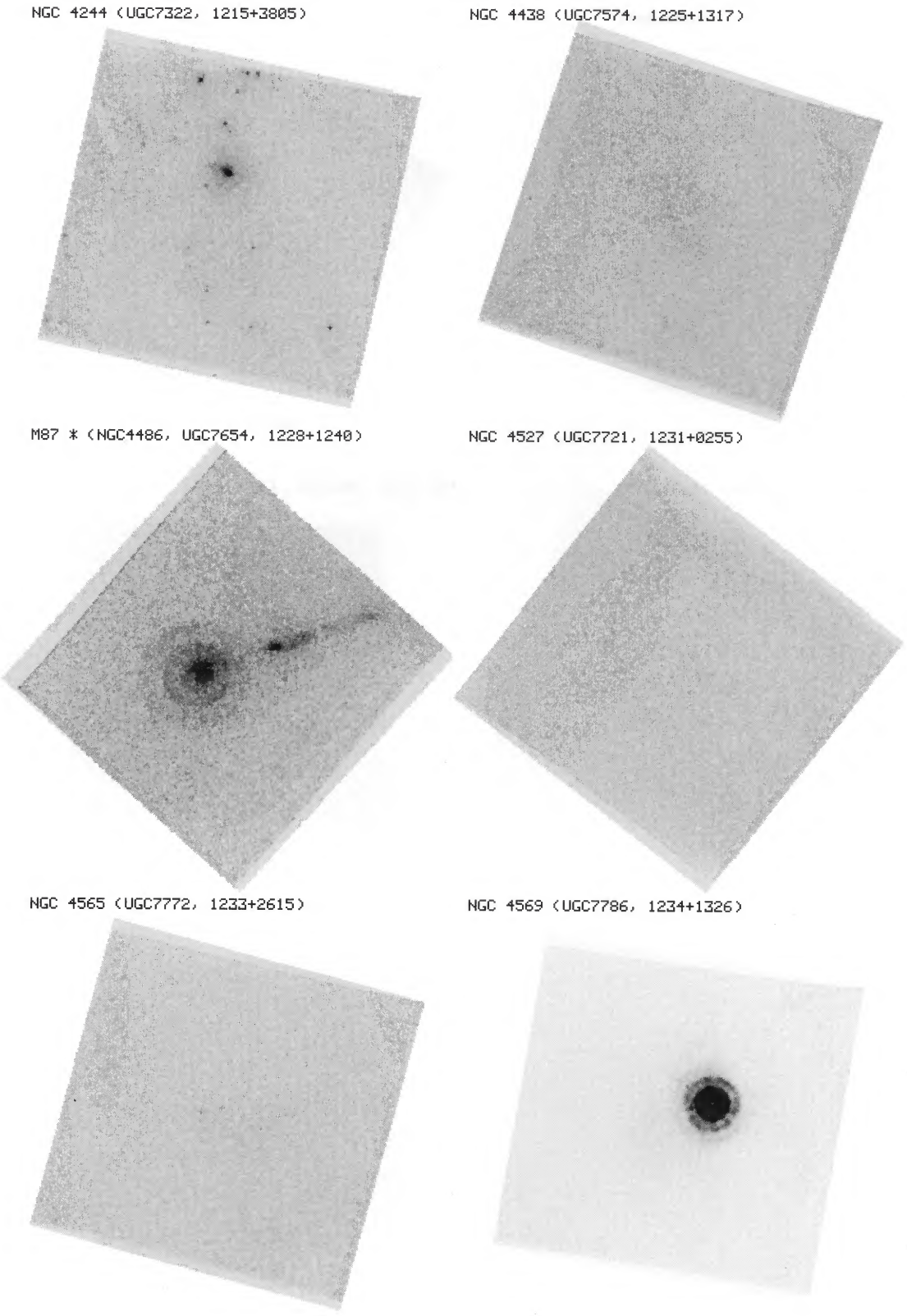

FIG. 2.—*Continued*

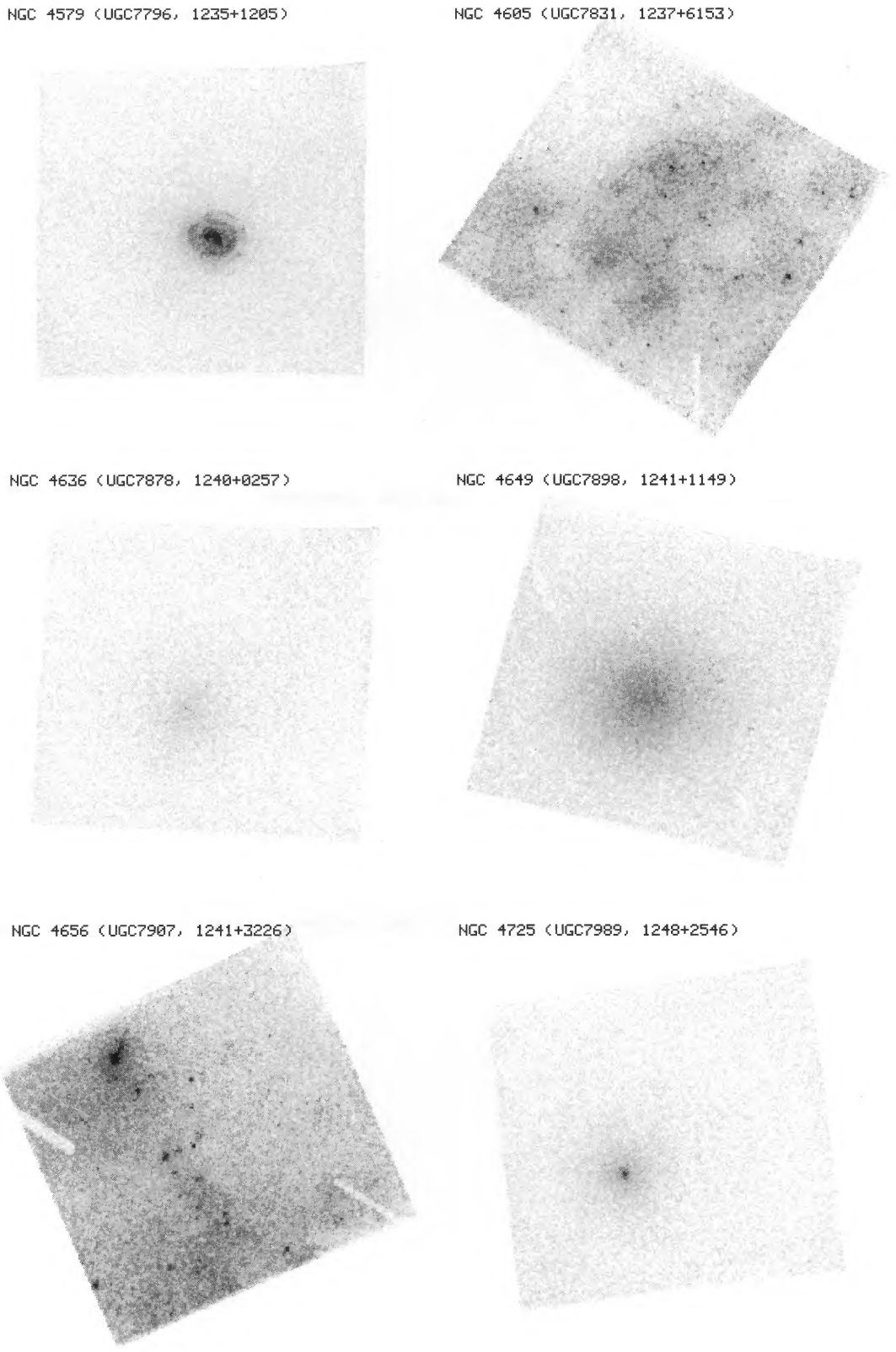

FIG. 2.—*Continued*

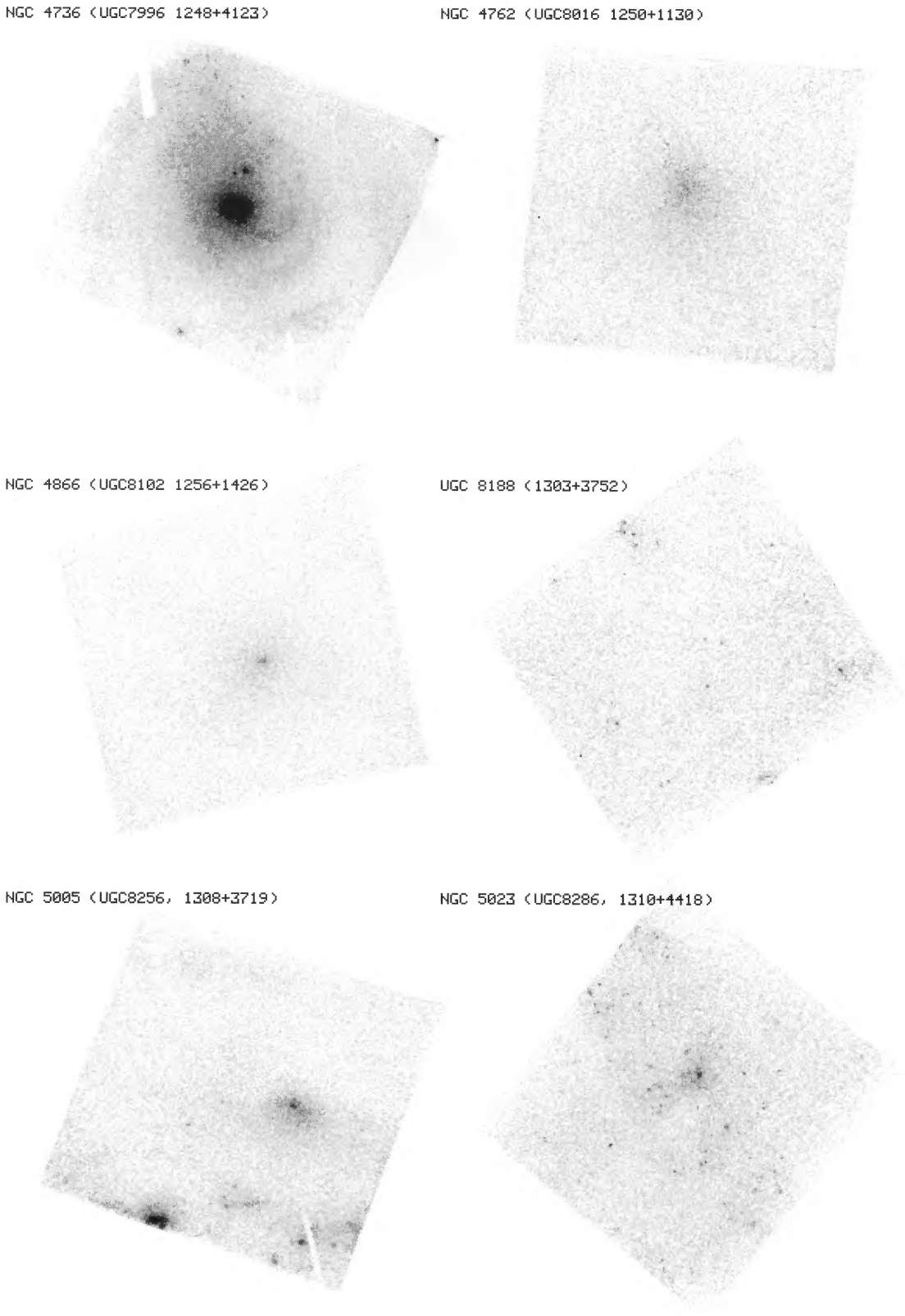

FIG. 2.—*Continued*

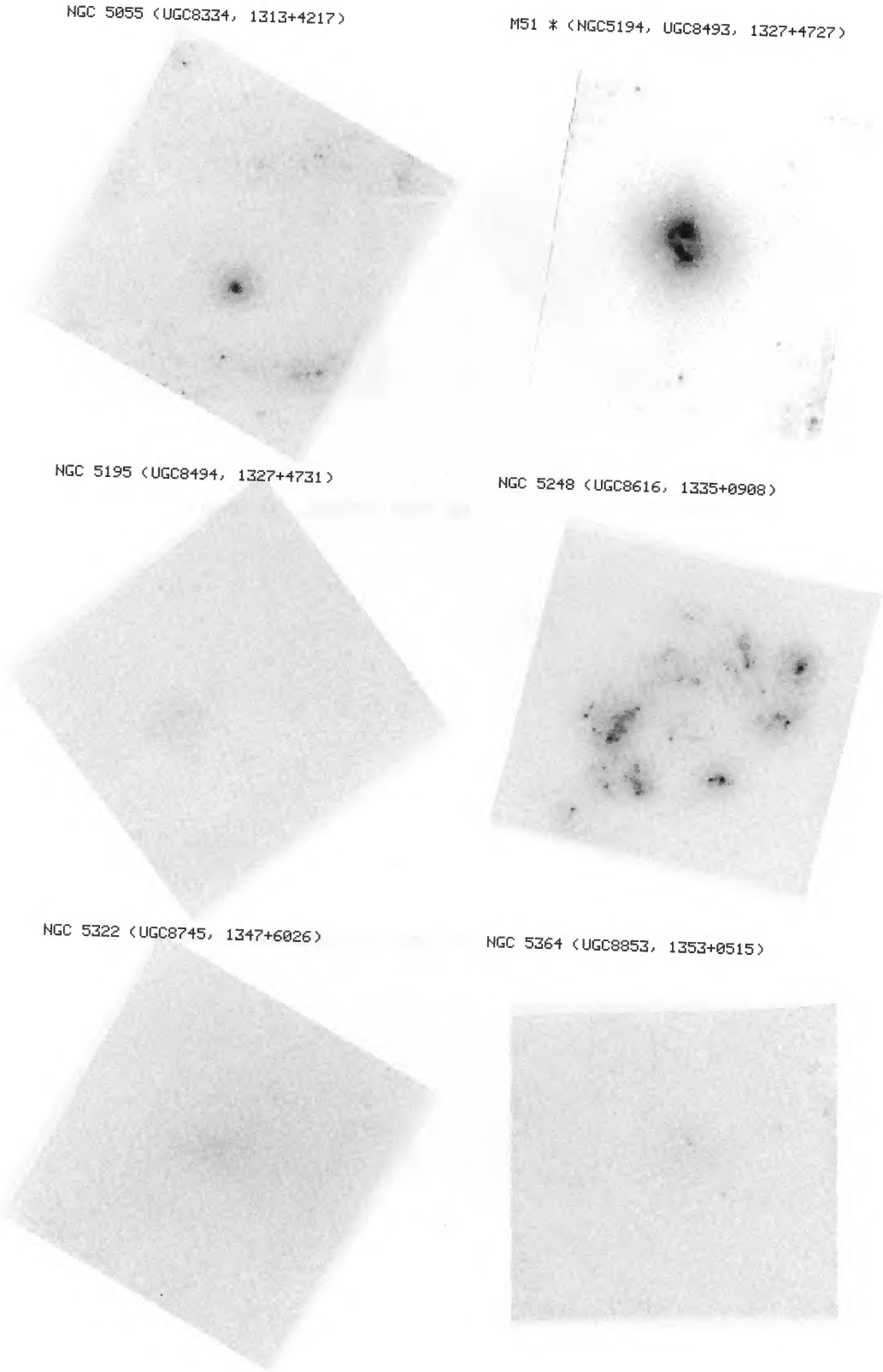

FIG. 2.—*Continued*

MAOZ et al. (see 107, 221)

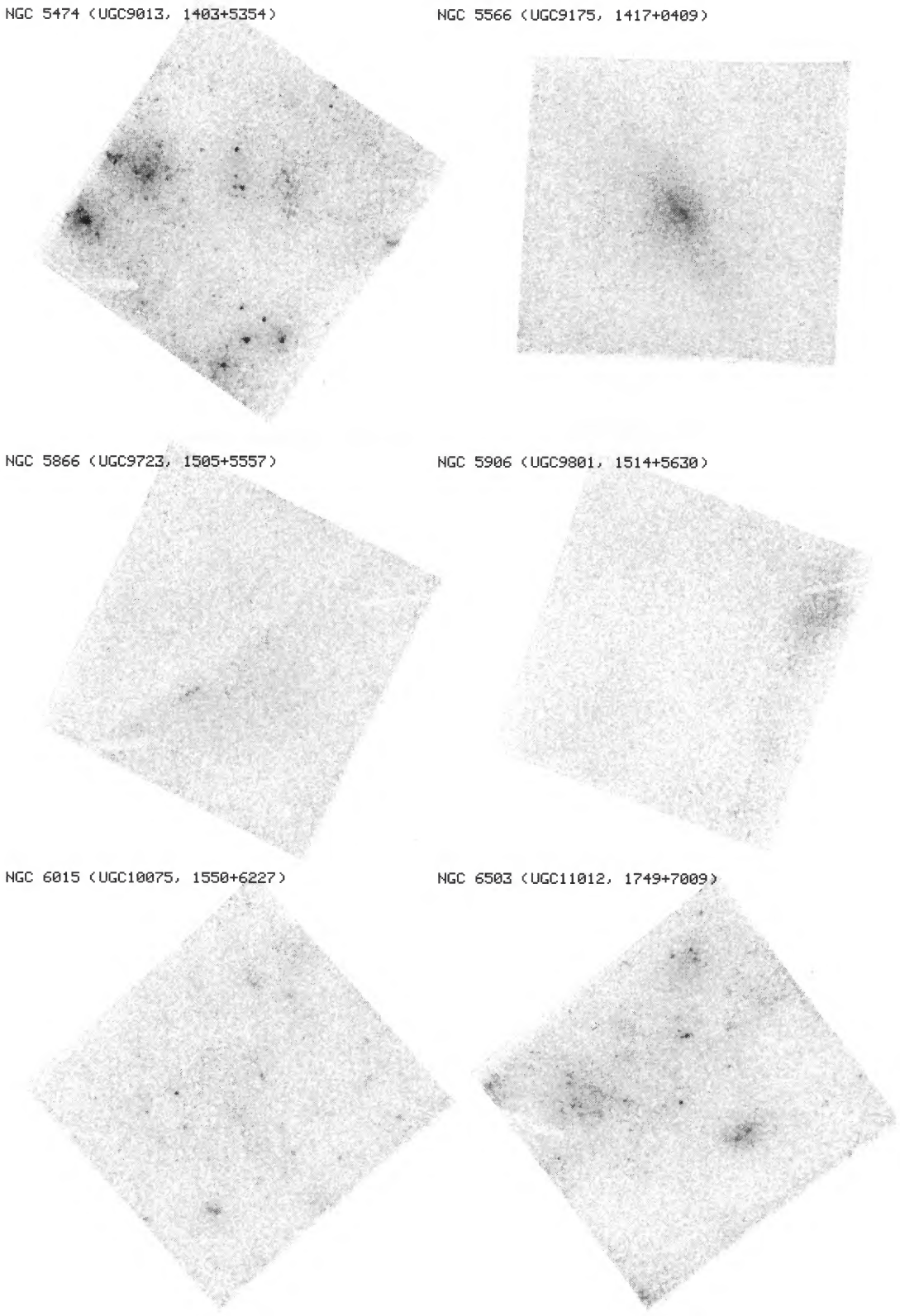

FIG. 2.—*Continued*

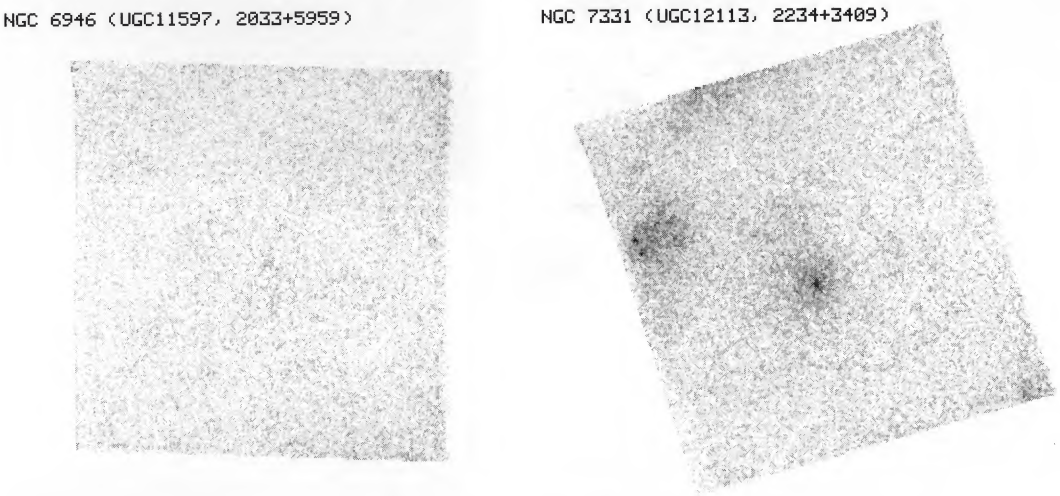

FIG. 2.—*Continued*

S0 galaxy was discovered by this survey. A detailed study, including rotation curves along the major axis and photometry of the compact young star clusters that contribute much of the UV light, can be found in Maoz et al. (1996).

NGC 1291 (0315−4117).—The central peak of the diffuse UV-light distribution may be unresolved in this SBa galaxy.

NGC 1332 (0324−2130).—This is an inclined S0 galaxy. A thin, unresolved dust lane crosses the diffuse light distribution about 0.″3 northeast of the central peak from southeast to northwest, along the orientation of the galaxy's major axis.

NGC 1385 (0335−2440).—This is a disturbed-looking Scd galaxy. The field of view includes part of some large structure, possibly the western spiral arm of the galaxy, that is bright in the UV and includes compact sources and diffuse emission. The UV-dark northern portion of the image is at the end of a large dusty spiral arm that crosses the northern part of the galaxy in optical images. The nuclear position is difficult to determine in optical images, and the bright knot on the western side of the UV image could be the galaxy nucleus.

NGC 1433 (0340−4722).—The circumnuclear star-forming ring seen in the UV image of this SBb galaxy is studied in detail by Maoz et al. (1996).

NGC 1512 (0402−4329).—The circumnuclear star-forming ring seen in the UV image of this SBb galaxy is studied in detail by Maoz et al. (1996); ∼40% of the UV light comes from compact young star clusters distributed along the ring. About 25% of the UV light is from the single bright "super star cluster" on the southeast side, which has an observed UV luminosity $L_\lambda(2300\ \text{Å}) \approx 10^{37}$ ergs s^{-1} Å^{-1} and a radius of only 2–3 pc.

NGC 1543 (0411−5751).—The UV image of this SB0/a galaxy shows a centrally peaked diffuse light distribution with an unresolved core or a faint central point source.

ESO 0450−2519.—The single weak source detected in this diffuse late-type spiral galaxy is unresolved or marginally resolved.

NGC 2997 (0943−3057).—This circumnuclear star-forming ring is studied in detail by Maoz et al. (1996). Utilizing also a *V*-band *HST* exposure of this galaxy, they show that the numerous compact (few pc radius) sources distributed along the ring are most probably young (less than 100 Myr) and massive ($\sim 10^5\ M_\odot$) clusters of stars that are gravitationally bound. These clusters, which appear similar to those in the many galaxies with S-type UV morphology presented here, may therefore evolve into objects similar to globular clusters.

NGC 4976 (1305−4914).—The UV image of this bright S0 galaxy shows only a faint, centrally peaked diffuse light distribution with an unresolved core or a weak central point source.

NGC 5084 (1317−2133).—The UV image of this S0 galaxy shows only a faint, centrally peaked diffuse light distribution with an unresolved core or a very weak central point source, with flux of order a few 10^{-18} ergs s^{-1} cm^{-2} Å^{-1}.

NGC 5102 (1319−3622).—The archival UV image of this nuclear-starburst S0 galaxy (e.g., Bica & Alloin 1987) is a 1137 s F220W exposure with the 512 × 512 pixel f/96 FOC format, which gives a field of view of 10″ × 10″. A bright, unresolved central point source is evidenced by the saturated central pixels and the sharp diffraction rings, surrounded by a high surface-brightness elliptical light distribution with major axis oriented northeast to southwest. A linear structure, probably an edge-on disk, can be traced out to about 1″ from the nucleus on both sides along the same direction.

NGC 5253 (1337−3123).—This nearby (4.1 Mpc; Sandage et al. 1994) starburst galaxy has been studied from radio to X-ray wavelengths, including *IUE* UV spectroscopy, which has revealed Wolf-Rayet spectral features (see Kinney et al. 1993, and references therein, for a summary). The FOC image presented here has been extensively studied by Meurer et al. (1995). This archival *HST* image is a 500 s exposure with the F220W filter plus a F1ND neutral-density filter, which provides a factor 2.5 attenuation in flux. The exposure is therefore one-third as deep as our standard-setup exposures. Nevertheless, the image shows numerous bright sources. As shown by Meurer et al. (1995), these are compact young star clusters of the type detected with *HST* in other starburst environments, as well as individual stars. This galaxy has the highest total UV flux in the sample.

ESO 2159−5132.—The image of this nearby irregular galaxy shows a large number of compact sources, most of which are probably individual O and B stars.

NGC 7462 (2260−4106).—The compact sources and diffuse emission in this nearly edge-on Sc galaxy are concentrated in a narrow strip running approximately east-west, along the galaxy's major axis.

ESO 2333−3903.—This faint but strongly nucleated Sd galaxy has an unresolved (FWHM < 0.″1) and weak central UV source, with a 2300 Å flux $\sim 1 \times 10^{-16}$ ergs s^{-1} cm^{-2} Å^{-1}.

3.3.2. *Northern Galaxies*

M31 (NGC 224, UGC 454, 0040+4100).—This archival image of the center of the Andromeda galaxy is one of three exposures described in detail by King et al. (1992) and King, Stanford, & Crane (1995). It is a 1677 s exposure with the f/48 FOC in its 512 × 1024 "zoomed" pixel mode, providing a 44″ × 44″ field of view. The filter is F175W, the peak transmission of which is at ∼1900 Å. Considering the response of this setup and the exposure time, the image is similar in sensitivity to the standard setup. The image shows bright, centrally peaked diffuse emission that is asymmetric at its peak. King et al. (1995) show that this peak coincides with the fainter of two peaks seen in optical *HST* images and with the dynamical center of the galaxy (Lauer et al. 1993). Many individual stars are also visible, and are discussed in detail by King et al. (1992).

NGC 404 (UGC 718, 0106+3527).—This S0 galaxy contains one of the UV-bright LINERs studied in detail by Maoz et al. (1995), showing a prominent unresolved nuclear point source.

NGC 672 (UGC 1256, 0145+2711).—The image of this Scd galaxy shows a resolved (FWHM ≈ 0.″2) central source plus several additional faint compact sources.

NGC 1023 (UGC 2154, 0237+3850).—This is an SB0 galaxy that has also been observed with *IUE* (Kinney et al. 1993). The integrated flux from the weak, centrally concentrated diffuse emission seen in the *HST* image agrees well with the *IUE* 2300 Å flux. This galaxy has also been imaged with *HST* by Lauer et al. (1995) in the *V* band, where it displays an unusually high central surface brightness. After deconvolution with the spherically aberrated PSF, they esti-

mate a surface brightness of 12.7 mag arcsec^{-2} in the central 0.″022 and 13.8 mag arcsec^{-2} at the 0.″1 radius. As in the other 45 early-type galaxies they have studied, the brightness profile continues to increase with decreasing radius all the way down to the *HST* angular resolution limit. The weak emission we detect from this galaxy in the UV, compared with the high visual surface brightness, confirms that the red leak through the F220W filter makes a negligible contribution to the counts we detect in the UV in other objects (see § 2 and notes on NGC 4636, below).

NGC 1560 (UGC 3060, 0427+7146).—The absence of UV flux from this galaxy may be due in part to its low Galactic latitude (+16°), at which a factor ~5 extinction in 2300 Å flux is expected (Burstein & Heiles 1982).

NGC 2903 (UGC 5079, 0929+2143).—This "hot-spot" Sc galaxy has been observed with *IUE*, and its spectrum indicates the presence of a mixture of early-type and late-type stars (Kinney et al. 1993). The *HST* image shows many bright compact sources, presumably young star clusters.

NGC 3079 (UGC 5387, 0958+5555).—There is very little UV emission detected in the image of this LINER galaxy. There is a hint of a dust lane crossing the image from north to south, at an orientation matching that of the galaxy's major axis.

NGC 3319 (UGC 5789, 1036+4156).—The elongated diffuse emission in the UV image is aligned with the strong bar of this Scd galaxy. There is an unresolved (FWHM < 0.″1) nuclear source with $f_\lambda(2300\ \text{Å}) = 1.4 \times 10^{-16}$ ergs s^{-1} cm^{-2} Å^{-1}, and several faint compact sources.

NGC 3344 (UGC 5840, 1040+2511).—This starburst nucleus has a bright unresolved nuclear point source and has been studied in more detail by Maoz et al. (1995).

NGC 3368 (UGC 5882, 1044+1205).—The UV image of this bright Sab LINER galaxy has a single, unresolved compact source with $f_\lambda(2300\ \text{Å}) \sim 5 \times 10^{-17}$ ergs s^{-1} cm^{-2} Å^{-1} about 0.″1 north of the centroid of a weak diffuse light distribution. We have verified by means of a ground-based CCD image that the source is at the galaxy's nucleus position. It is 5.″5 south of the center of the image because the galaxy nucleus coordinates input to *HST* were off by that much due to galaxy isophote distortion by a dust lane in the GASP image. This is another example of a "UV-bright" LINER (Maoz et al. 1995), though with a central point source fainter by 1–2 orders of magnitude. In contrast to the other UV-bright LINERs, the observed UV fluxes of which are sufficient to explain their observed emission-line fluxes by photoionization, in this source the observed UV flux is 20 times less than the minimum required (see Maoz 1996). This LINER is therefore reddened or not excited through photoionization and could be an intermediate case between UV-bright and UV-dark.

NGC 3486 (UGC 6079, 1057+2914).—There is a weak ($f_\lambda(2300\ \text{Å}) = 1 \times 10^{-16}$ ergs s^{-1} cm^{-2} Å^{-1}), unresolved (FWHM < 0.″1) point source in the nucleus of this galaxy, which is a LINER/weak-Seyfert 2 (Ho et al. 1996a). The Hα flux measured by Ho et al. (1996a) is about 1×10^{-14} ergs s^{-1} cm^{-2}. Using the argument of Maoz et al. (1995) and Maoz (1996) in the cases of other LINERs in the sample, a power-law extrapolation beyond the Lyman limit of the observed UV flux provides enough ionizing photons to explain the observed Hα flux through photoionization in this object as well. The central point source could therefore be the AGN continuum source.

NGC 3521 (UGC 6150, 1103+0014).—The central diffuse light distribution in the UV image of this Sbc galaxy has a double-peaked appearance, apparently because it is crossed by an obscuring dust feature. The feature is reminiscent of the X-shaped dust lanes in M51 (NGC 5194; see below), but this requires confirmation with data of higher signal-to-noise ratio (S/N).

NGC 3627 (UGC 6346, 1117+1315).—The nucleus of this bright Sb galaxy has a prominent optical emission-line spectrum that is intermediate between that of a LINER and and an H II nucleus (Ho et al. 1996a). The UV image shows a weak, diffuse centrally peaked light distribution. It is offset from the image center because of an inaccuracy in the nuclear position that was estimated from a GASP image and input to *HST*. There is a hint of spiral structure which, however, requires confirmation.

NGC 3718 (UGC 6524, 1129+5320).—This Sa galaxy has a prominent optical LINER spectrum, including a broad Hα component similar to that of Seyfert 1 galaxies (Ho et al. 1996a). Its UV image is blank, and this may be related to the fact that the optical line ratios are indicative of reddening. A dust lane that crosses optical images of the galaxy near the nucleus is a candidate agent of these effects.

NGC 4151 (UGC 7166, 1208+3941).—This is probably the best studied Seyfert 1 galaxy. The archival image is a 900 s exposure with the f/48 FOC in its 512 × 1024 "zoomed" pixel mode. The image was taken after the *HST* refurbishment mission and the installation of COSTAR, and so is free of spherical aberration. The field of view is 28″ × 28″, with a dezoomed pixel size of 0.″014. The image was obtained with a combination of the F220W and F275W filters, giving an effective peak transmission at ~2450 Å. Considering the response of this setup and the exposure time, the image has one-fourth the sensitivity of the standard setup for diffuse sources, but better sensitivity to compact sources because of the improved optics. The bright Seyfert 1 nucleus is strongly saturated. Its brightness cannot be reconstructed, as in Maoz et al. (1995), because of the absence of the spherical-aberration diffraction rings. In addition to the nuclear point source, there is a diffuse-light distribution centered 2″ south of the nucleus. Excluding the counts from the central source, the flux from the diffuse component is 1.2×10^{-13} ergs s^{-1} cm^{-2} Å^{-1}. This value casts doubt on the component's reality since measurements with *IUE*, the aperture of which would include much of this extended (and presumably nonvariable) emission, have been at times up to a factor of 6 lower at this wavelength (e.g., Ulrich et al. 1991). The diffuse component may be an artifact of the poor quality of the f/48 FOC flat field, or of a dark current in this camera, which has had operational problems since 1992 December. The large arc to the west is an artifact.

NGC 4192 (UGC 7231, 1211+1510).—This highly inclined Sb galaxy has a nucleus with strong optical emission lines, with line ratios intermediate between a LINER and an H II nucleus, and indicative of reddening (Ho et al. 1996a). Its UV image shows three amorphous knots of very weak emission.

NGC 4214 (UGC 7278, 1213+3637).—This starburst Magellanic irregular galaxy has been studied in the UV with *IUE* (Huchra et al. 1983; Hartmann, Geller, & Huchra 1986) and in the optical (Sargent & Filippenko 1991) and shows Wolf-Rayet signatures. The archival *HST* FOC image shown here is analyzed, along with *HST* spectroscopy, by Leitherer et al. (1996). It is a 1200 s exposure with

the standard format, but with a F2ND neutral density filter, which attenuates the flux by a factor of 5, in addition to the F220W filter. The sensitivity is then 0.4 times that of the standard setup. The image shows a bright central point source, surrounded by numerous compact sources. Most of the total UV flux, which is in excellent agreement with that measured by *IUE* at 2300 Å (Kinney et al. 1993), comes from the central source. Leitherer et al. (1996) argue that most of the fainter sources are individual stars. This galaxy has the second largest total UV flux in the sample (after NGC 5253).

NGC 4438 (UGC 7574, 1225+1317).—The UV image of this S0 galaxy shows only a weak amorphous patch of UV emission, about 5″ in size. Filippenko & Sargent (1985) note that the strong LINER-like emission that is seen in optical spectra comes from an extended region.

M87 (NGC 4486, UGC 7654, 1228+1240).—This is the central elliptical galaxy in the Virgo cluster and a much-studied AGN, with a LINER nucleus and a jet that is visible at radio, optical, and UV wavelengths. UV images of the nucleus and the jet have been previously published by Boksenberg et al. (1992). This archival image is a 1200 s exposure with the FOC/96 in its "normal" (i.e., unzoomed) 512 × 512 pixel format, giving a 10″ × 10″ field of view, and the standard F220W filter. The exposure is 1.6 times more sensitive than the standard setup. The image shows a bright central point source, and the knots of the UV jet emerging westward. The UV flux from the central point source, 1×10^{-15} ergs s^{-1} cm^{-2} $Å^{-1}$, is sufficient to provide the observed Hα flux through photoionization, as in the other UV-bright LINERs in the sample (Maoz et al. 1995; Maoz 1996).

NGC 4569 (UGC 7786, 1234+1326).—This Sab galaxy contains one of the UV-bright LINERs studied in more detail by Maoz et al. (1995). Apart from the bright unresolved nuclear point source, there is some faint extended emission 0.″65 south of the nucleus.

NGC 4579 (UGC 7796, 1235+1205).—This is one of the UV-bright LINERs studied in more detail by Maoz et al. (1995), showing a bright unresolved nuclear point source. The main source is surrounded by several fainter sources, giving the diffraction rings in the image their asymmetric appearance.

NGC 4636 (UGC 7878, 1240+0257).—This E/S0 galaxy has an optical LINER spectrum, with broad Hα wings (Ho et al. 1996a). The UV image shows diffuse, centrally concentrated emission. This galaxy has also been imaged with *HST* by Lauer et al. (1995) in the *V* band, where it shows similar structure. The *V*-band brightness profile increases with decreasing radius down to the *HST* resolution, though with a shallower slope than most of the other early-type galaxies studied by Lauer et al. (1995). They estimate (after deconvolution with the spherically aberrated PSF) a surface brightness of 16.5 mag $arcsec^{-2}$ in the central 0.″022, and 16.7 mag $arcsec^{-2}$ at the 0.″1 radius. The comparable UV brightnesses of this galaxy and NGC 1023 (which was also imaged by Lauer et al. 1995), despite the much higher optical surface brightness of NGC 1023, confirms that the red leak through the F220W filter contributes negligibly to the counts in the FOC exposures, and that most of the signal detected in the FOC exposures is, in fact, the result of UV flux (see § 2 and notes on NGC 1023).

NGC 4725 (UGC 7989, 1248+2546).—This bright SBb galaxy hosts a weak Seyfert 2 nucleus (Ho et al. 1996a). The UV image shows a diffuse centrally peaked light distribution, with a marginally resolved core of width ≈0.″2.

NGC 4736 (UGC 7996, 1248+4123).—This ringed Sab galaxy has many peculiar features, suggesting it is in the final stages of a merger. It is one of the UV-bright LINERs studied in more detail by Maoz et al. (1995) and has two bright unresolved UV point sources, one on the nucleus and one 2.″5 to the north. Using the algorithm of Maoz et al. (1996), we measure for the nuclear point source a UV flux density $f_\lambda(2300\ Å) = 1.9 \times 10^{-16}$ ergs s^{-1} cm^{-2} $Å^{-1}$ and for the northern source $f_\lambda(2300\ Å) = 2.6 \times 10^{-16}$ ergs s^{-1} cm^{-2} $Å^{-1}$. The nuclear point source sits on top of a high surface-brightness diffuse component that extends into a number of concentric arcs. Several fainter compact sources are also visible.

NGC 4866 (UGC 8102, 1256+1426).—The UV image of this Sa galaxy, the nucleus of which has a LINER spectrum (Ho et al. 1996a), shows a weak, centrally peaked diffuse light distribution. There is a hint of a dust lane crossing the nucleus in the UV image, but this needs confirmation with higher S/N.

NGC 5005 (UGC 8256, 1308+3719).—This is a bright Sbc galaxy with a LINER nucleus (Ho et al. 1996a). We have compared the gross features of the UV image to a narrowband ground-based Hα image and verified that the faint diffuse emission that appears several arcseconds west of the center in the UV image is in fact the nucleus of the galaxy. The knot of UV sources on the southeast edge of the image corresponds in the ground-based image to an Hα knot. There may be a very faint compact V-shaped source of UV emission on top of the diffuse nuclear emission, but this requires confirmation at higher S/N.

NGC 5055 (UGC 8334, 1313+4217).—This is one of the UV-bright LINERs studied in more detail by Maoz et al. (1995), showing a bright marginally resolved nuclear point source. Many fainter compact sources are also visible in the northern and southern corners of the image.

M51 (NGC 5194, UGC 8493, 1327+4727).—This face-on Sbc Seyfert 2 galaxy forms an interacting pair with NGC 5195 and has been the focus of many studies. The archival *HST* image is a 2277 s exposure with the f/96 FOC in its "normal" (i.e., unzoomed) 512 × 512 pixel format, giving a 10″ × 10″ field of view, and the F275W filter, at an effective wavelength ∼2800 Å. The longer wavelength and exposure time make this image about 8 times more sensitive than the standard setup. The image shows X-shaped dust lanes crossing the bright diffuse light distribution, previously noted in visual-band *HST* images (Ford et al. 1992; see Maran & Kinney 1993) and a number of compact sources on the outskirts of the field.

NGC 5195 (UGC 8494, 1327+4731).—This is the companion galaxy interacting with M51 (NGC 5194). The UV image is nearly blank, with only some faint diffuse emission.

NGC 5248 (UGC 8616, 1335+0908).—This Sbc galaxy contains one of the circumnuclear star-forming rings studied in detail by Maoz et al. (1996).

NGC 5322 (UGC 8745, 1347+6026).—This is an E4 elliptical galaxy with a weak LINER nucleus (Ho et al. 1996a). The UV image shows weak, diffuse, centrally concentrated structure that is elongated in the east-west direction, like the galaxy's major axis in optical images. A pre-COSTAR *HST V*-band image of the galaxy (Lauer et al. 1995) shows similar structure and also a thin dust lane crossing the nucleus. There is a hint of this dust lane, also in

the east-west direction, in the UV image.

NGC 5474 (UGC 9013, 1403+5354).—This Scd galaxy is one of a group that is tidally interacting with the large galaxy M101 (NGC 5457; Kinney et al. 1993). The image shows many compact sources, presumably young star clusters and individual O and B stars.

NGC 5866 (UGC 9723, 1505+5557).—The UV image of this S0 galaxy displays weak, amorphous emission. The optical spectrum of the nucleus is a "transition type" between LINER and H II, with weak broad Hα wings (Ho et al. 1996a).

NGC 6946 (UGC 11597, 2033+5959).—This is a well-known low-surface-brightness, face-on, Scd starburst galaxy (e.g., DeGioia-Eastwood 1985; Devereux & Young 1993). The absence of UV flux in the FOC exposure may be due in part to its low Galactic latitude (+12°), at which a factor ~5 extinction in 2300 Å flux is expected (Burstein & Heiles 1982).

NGC 7331 (UGC 12113, 2234+3409).—This bright Sb galaxy has the optical spectrum of a "transition object" between a LINER and an H II nucleus (Ho et al. 1996a). The UV image shows a faint but strongly peaked diffuse light ditribution and some additional emission on the eastern edge of the field.

4. SUMMARY

We have presented *HST* UV images of the central regions of 110 large nearby galaxies. The observed galaxies are an unbiased selection from a complete sample of all large and nearby galaxies. This is the first such UV imaging survey of normal galaxies. The images display an assortment of morphologies and UV brightnesses. These include bright unresolved (<0.″1, usually corresponding to a few pc) nuclear point sources, compact young star clusters scattered in the field or arranged in circumnuclear rings, centrally peaked diffuse light distributions, and galaxies with weak or undetected UV emission. For every galaxy, we have measured the integrated ~2300 Å flux, classified the UV morphology, and tabulated these parameters along with others from the literature.

From comparing the galaxy parameters, the following trends emerge. As seen in Figure 3, the centrally peaked diffuse (F-type) UV morphology tends to occur in spirals earlier than type Sc, and in S0s and ellipticals. This UV morphology is therefore the signature of a spheroidal population, although not all spheroids produce it. Galaxies with this morphology tend to have a lower UV flux, integrated over the central 20″, than others. The central UV flux of the F-types is not correlated with the integrated *B* magnitude of the entire galaxy. However, there are no galaxies in the sample fainter than $B \approx 12$ mag with an F-type morphology (or, for that matter, with a nuclear point source [P]). The latter three properties can be seen in Figure 4.

Conversely (see Fig. 3), the star-forming (S-type) UV morphology tends to occur more in late-type galaxies, but it can be found in all Hubble types. The highest integrated central UV fluxes occur in galaxies with S-type morphology although, again, a large range in flux exists. In these S-types, the central UV flux is correlated with the galaxy's integrated *B* magnitude, but with a large scatter. These trends are shown in Figure 4. Galaxies that are null (B) or weak (W) UV emitters do not have significantly fainter integrated *B* magnitudes than galaxies that are UV-bright. As already noted, the fraction of galaxies with B-type morphology that have an inclination greater than 60° is 10/13, as opposed to the 1/2 expected from a random ditribution (and which the other types obey). This suggests that dust in the disk of a nearly edge-on galaxy sometimes stifles completely what may have been a W-type emitter. On the other hand, the converse is not true; we find no trend of UV flux with axis ratio, and many highly inclined galaxies are plentiful UV emitters.

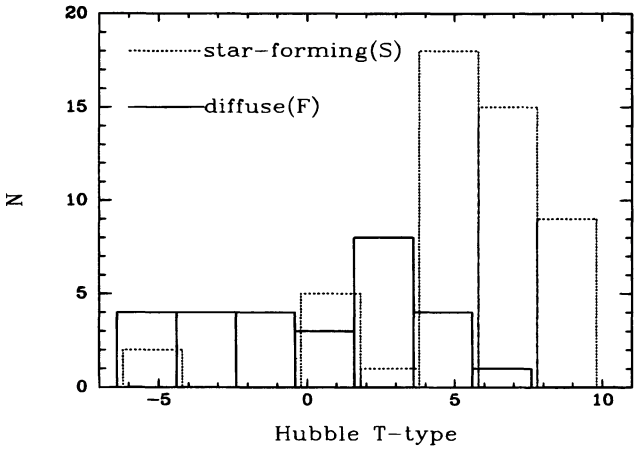

FIG. 3.—Distribution of galaxy Hubble types (labeled according to de Vaucouleurs's T-types) for galaxies with a star-forming (S-type; *dotted histogram*) UV morphology, and galaxies with a diffuse centrally peaked (F-type; *solid histogram*) UV morphology. F-types tend to occur in earlier type galaxies and are apparently associated with a galaxy spheroid. S-type UV morphologies are found preferentially in the centers of late-type spirals but can occur in all Hubble types.

Comparing the northern sample's UV properties to the optical spectral classification of Ho et al. (1996a), we find that galaxies with a star-forming (S) UV morphology never have a "pure" LINER-type (L) spectrum. This is as expected, since the UV sources in the S-types are probably young star clusters or individual O and B stars, the ionization of which will add H II–like spectral features to a LINER spectrum. Also, galaxies with a nuclear point source are never devoid of emission lines in the optical spectrum

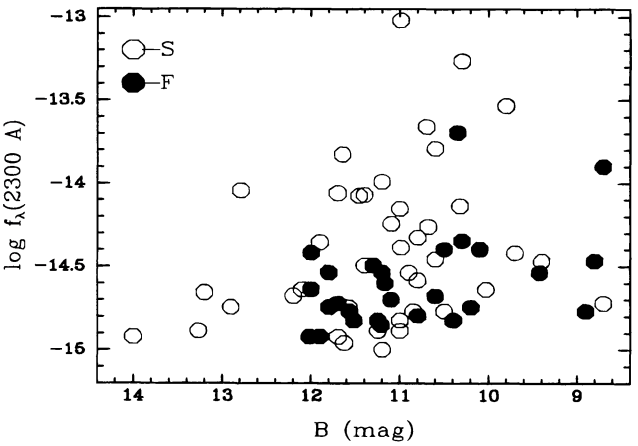

FIG. 4.—Observed flux density at 2300 Å integrated over the central 22″ × 22″ of each galaxy vs. *B* magnitude integrated over the whole galaxy, for galaxies with F-type UV morphologies (*filled circles*) and S-type UV morphologies (*open circles*). The central UV flux of F-types is uncorrelated with the galaxy's integrated *B* magnitude, but such a morphology is found in the sample only in galaxies brighter than $B = 12$ mag. For S-types, on the other hand, the central UV flux appears to be loosely correlated with the total *B* magnitude. The typical UV flux from F-types is several times lower than that of S-types, which have the highest UV fluxes in the sample.

(spectral classification "A") suggesting that, if a nuclear UV continuum source is present, there is usually enough gas in the nucleus to be ionized by it and produce emission lines. As shown in Figure 5, the highest central UV fluxes are measured in galaxies with an H II–like (H-class) optical spectrum, and the median UV flux of this class is several times higher than that of galaxies with the other types of nuclear spectra. This is also not surprising, since Ho et al. (1996a) show that such spectra tend to occur in late-type galaxies, and we have found (see above) that these are the Hubble types with the highest UV fluxes.

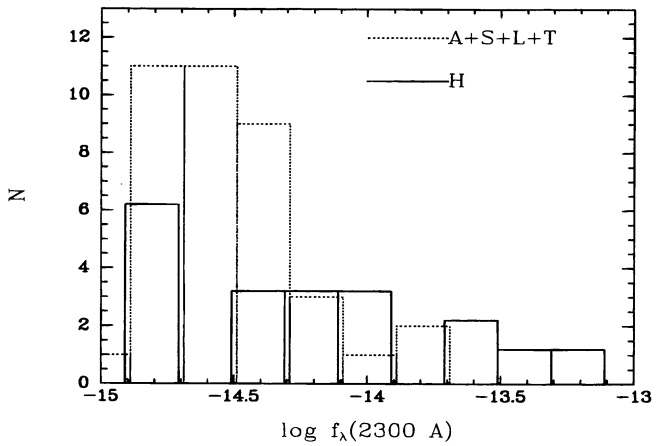

FIG. 5.—Distribution of central UV flux density, as observed with the FOC, for galaxies with an H II–like optical nuclear spectrum (H-type spectral classification; *solid histogram*) and galaxies with other optical nuclear classifications (absorption, A; Seyfert, S; LINER, L; or transition-type, T; *solid histogram*). Galaxies with H II-like optical nuclear spectra tend to have higher integrated central UV flux, and the galaxies with the highest UV fluxes are of this type.

The data we have presented can be useful for studying star formation and low-level nuclear activity in galaxies, for identifying galaxies with significant "UV-upturn" emission from an evolved stellar population, and for searching for interconnections between these phenomena. These are the subjects of recent and forthcoming publications based on this survey.

We are grateful to J. N. Bahcall for his contribution to the earlier stages of this survey, to T. Lauer for providing information on the central surface brightness of two early-type galaxies, and to the referee, A. Sandage, for constructive comments. This work was supported by grant GO-3519 from the Space Telescope Science Institute, which is operated by AURA, Inc., under NASA contract NAS 5-26555. A. V. F. and L. C. H. also acknowledge support by grant AR-4911 from the Space Telescope Science Institute. D. M. and H.-W. R. acknowledge support by the US-Israel Binational Science Foundation grant 94-00300.

REFERENCES

Baxter, D. A., Gilmore, D., Greenfield, P. E., Hack, W., Hodge, P., Jedrzejewski, R. I., & Nota, A. 1994, in *HST* Data Handbook, ed. S. Baum (Baltimore: STScI), 123
Benvenuti, P., Macchetto, F. D., & Schreier, E. J. 1996, Science with the *Hubble Space Telescope* (Baltimore: STScI), in press
Bica, E., & Alloin, D. 1987, A&AS, 70, 281
Bohlin, R. C., Cornett, R. H., Hill, J. K., O'Connell, R. W., & Stecher, T. P. 1990, ApJ, 352, 55
Boksenberg, A., et al. 1992, A&A, 261, 393
Burrows, C. J., et al. 1991, ApJ, 369, L21
Burstein, D., Bertola, F., Buson, L. M., Faber, S. M., & Lauer, T. R. 1988, ApJ, 328, 440
Burstein, D., & Heiles, C. 1982, AJ, 87, 1165
Conti, P. S., & Vacca, W. D. 1994, ApJ, 423, L97
DeGioia-Eastwood, K. 1985, ApJ, 288, 175
de Vaucouleurs, G., de Vaucouleurs, A., Corwin, H. G., Buta, R. J., Paturel, G., & Fouqué, P. 1991, Third Reference Catalog of Bright Galaxies (New York: Springer)
Devereux, N. A., & Young, J. S. 1993, AJ, 106, 948
Filippenko, A. V., & Sargent, W. L. W. 1985, ApJS, 57, 503
———. 1986, in Structure and Evolution of Active Galactic Nuclei, ed. G. Giuricin et al. (Dordrecht: Reidel), 21
Ford, H. C., Caganoff, S., Kriss, G. A., Tsvetanov, Z., & Evans, I. N. 1992, BAAS, 180, 5403
Hartmann, L. W., Geller, M. J., & Huchra, J. P. 1986, AJ, 92, 1278
Hill, J. K., Isensee, J. E., Bohlin, R. C., O'Connell, R. W., Roberts, M. S., Smith, A. M., & Stecher, T. P. 1992, ApJ, 414, L9
Ho, L. C., Filippenko, A. V., & Sargent, W. L. W. 1995, ApJS, 98, 477
———. 1996a, in preparation
Ho, L. C., et al. 1996b, in preparation
Huchra, J. P., Geller, M. J., Gallagher, J., Hunter, D., Hartmann, L., Fabbiano, G., & Aaronson, M. 1983, ApJ, 274, 125
King, I. R., et al. 1992, ApJ, 397, L35
King, I. R., Stanford, S. A., & Crane, P. 1995, AJ, 109, 164
Kinney, A. L., Bohlin, R. C., Calzetti, D., Panagia, N., & Wyse, R. F. G. 1993, ApJS, 86, 5
Kinney, A. L., Calzetti, D., Bohlin, R. C., McQuade, K., Storchi-Bergmann, T., & Schmitt, H. R. 1996, ApJ, 467, 38
Landsman, W. B., Roberts, M. S., Bohlin, R. C., O'Connell, R. W., Smith, A. M., & Stecher, T. P. 1992, ApJ, 401, L83
Lauberts, A., & Valentijn, E. A. 1989, The Surface Photometry Catalogue of the ESO-Uppsala Galaxies (Garching: ESO)
Lauer, T. R., et al. 1993, AJ, 106, 1436
———. 1995, AJ, 110, 2622
Leitherer, C., Vacca, W. D., Conti, P. S., Filippenko, A. V., Robert, C., & Sargent, W. L. W. 1996, ApJ, 465, 717
Maoz, D. 1996, in The Physics of LINERs in View of Recent Observations, ed. M. Eracleous, A. Koratkar, C. Leitherer, & L. C. Ho (Baltimore: STScI), 90
Maoz, D., Barth, A. J. Sternberg, A., Filippenko, A. V., Ho, L. C., Macchetto, F. D., Rix, H.-W., & Schneider, D. P. 1996, AJ, 111, 2248
Maoz, D., Filippenko, A. V., Ho, L. C., Rix, H.-W., Bahcall, J. N., Schneider, D. P., & Macchetto, F. D. 1995, ApJ, 440, 91
Maran, S. P., & Kinney, A. L. 1993, PASP, 105, 447
Meurer, G. R. 1995, Instrument Science Report FOC-083 (Baltimore: STScI)
Meurer, G. R., Heckman, T. M., Leitherer, C., Kinney, A., Robert, C., & Garnett, D. R. 1995, AJ, 110, 2665
Paresce, F. 1990, Faint Object Camera Instrument Handbook (Baltimore: STScI)
Sargent, W. L. W., & Filippenko, A. V. 1991, AJ, 102, 107
Sandage, A., Saha, A., Tammann, G. A., Labhardt, L., Schwengler, H., Panagia, N., & Macchetto, F. D. 1994, ApJ, 423, L13
Sandage, A., & Tammann, G. A. 1987, A Revised Shapley-Ames Catalog of Bright Galaxies, 2nd ed. (Washington DC: Carnegie Inst.)
Ulrich, M.-H., et al. 1991, ApJ, 382, 483